UNIVERSITAT POLITÈCNICA DE VALÈNCIA

Escola Tècnica Superior d'Enginyeria Agronòmica i del Medi Natural

UNIVERSITAT POLITÈCNICA DE VALÈNCIA

School of Agricultural Engineering and Environment

Development of Lipid Nanoparticles for Enzymatic Therapies

End of Degree Project

Bachelor's Degree in Biotechnology

AUTHOR: Blázquez Ruiz, Marta

Tutor: Llopis Lorente, Antoni

External cotutor: VENTURA COBOS, JORDI

Experimental director: BASTANTE RODRIGUEZ, DAVID

ACADEMIC YEAR: 2023/2024

UNIVERSITAT POLITÈCNICA DE VALÈNCIA

Escola Tècnica Superior d'Enginyeria Agronòmica i del Medi Natural

Instituto Interuniversitario de Investigación de Reconocimiento Molecular y Desarrollo Tecnológico

UNIVERSITAT POLITÈCNICA DE VALÈNCIA

Escuela Técnica Superior de Ingeniería Agronómica y del Medio Natural

Development of Horseradish Peroxidase-Loaded Liposomes for Enzyme-Based Cancer Therapy

Biotechnology Bachelor's Degree
Final Degree Project

2023/2024

Author: Marta Blázquez Ruiz

Tutor: Dr. Antoni Llopis Lorente
Academic co-tutor: Jordi Ventura Cobos
Experimental co-tutor: David Bastante Rodríguez

Valencia, April 2024

Development of Horseradish Peroxidase-Loaded Liposomes for Enzyme-Based Cancer Therapy

Abstract

Cancer is a complex disease with a significant global impact and high mortality rate due to the limited effectiveness of available treatments. Chemotherapy is one of the most used cancer treatment methods, relying on the non-selective destruction of rapidly dividing cells by drug administration, encompassing both tumor and healthy cells. Nanomedicine offers modern approaches in comparison to traditional anti-cancer methods, providing targeted drug delivery that avoids side effects and enhances drug therapeutics.

In this work, we present the design and evaluation of large unilamellar vesicles (LUVs) loaded with the enzyme horseradish peroxidase (HRP) for enzyme-prodrug therapy (EPT). HRP has shown potential for cancer treatment, as it produces reactive oxygen species (ROS) through oxidation of the prodrug indole-3-acetic acid (IAA). This oxidative stress leads to apoptosis. Liposomes were chosen as delivery nanoplatform as they present important characteristics such as biocompatibility, biodegradability, and low immunogenicity. Specifically, LUVs were selected due to their optimal size range, which promote cellular uptake and enables penetration through fenestrated vessels into tumor tissues. These fenestrated vessels, product of the defective angiogenesis of cancer cells proliferation, will enable enhanced permeability and retention effect (EPR), which will work as passive targeting mechanism. LUVs were prepared by thin-film hydration method and characterized by dynamic light scattering (DLS). The incorporation of HRP into LUVs (HRP-loaded LUVs) was achieved by hydration. HRP-LUVs were characterized by dynamic light scattering (DLS), nanoparticles tracking analysis (NTA) and transmission electron microscopy (TEM). Protein quantification and enzymatic activity assays were also conducted. Finally, preliminary cellular experiments were performed to evaluate biocompatibility of the HRP-loaded LUVs in *in vitro* culture of SK-Mel-103 melanoma cancer cells. The WST-1 assay was performed to evaluate cell viability. HRP-loaded LUVs showed good biocompatibility, which opens the possibility to evaluate their therapeutic properties in future studies. In conclusion, this work has successfully developed HRP-loaded liposomes and shows interesting prospects for their application as anticancer therapy.

Key words: liposomes, LUVs, cancer, nanomedicine, HRP, enzyme-prodrug therapy, EPT

Author: Marta Blázquez Ruiz
Tutor: Dr. Antoni Llopis Lorente
Academic co-tutor: Jordi Ventura Cobos
Experimental co-tutor: David Bastante Rodríguez

Valencia, April 2024

Desarrollo de Liposomas Cargados con Peroxidasa de Rábano Picante Para Terapias Enzimáticas Contra el Cáncer

Resumen

El cáncer es una enfermedad compleja, con un gran impacto a nivel mundial y una alta tasa de mortalidad debido a las limitaciones existentes de los tratamientos disponibles. La quimioterapia es uno de los tratamientos más comunes contra el cáncer, incluyendo su mecanismo la destrucción no selectiva de células, lo que afecta tanto a células cancerosas como a las sanas. La nanomedicina ofrece enfoques innovadores, permitiendo una administración selectiva de medicamentos que reduce los efectos secundarios y mejora la eficacia del tratamiento.

En este trabajo, se describe el diseño y la evaluación de vesículas unilamelares grandes (LUVs) cargadas con la enzima peroxidasa de rábano picante (HRP) para terapia enzima-profármaco (EPT). La HRP ha mostrado potencial en el tratamiento del cáncer al generar especies reactivas de oxígeno (ROS) mediante la oxidación del profármaco ácido indol-3-acético (IAA), lo que induce apoptosis. Optamos por los liposomas como plataforma nanotecnológica debido a su biocompatibilidad, biodegradabilidad y baja inmunogenicidad. Específicamente, elegimos LUVs por su adecuado tamaño, facilitando la captación celular y la penetración en tejidos tumorales a través de vasos fenestrados, típicos de la angiogénesis defectuosa en células cancerosas. Este fenómeno permite una mayor permeabilidad y efecto de retención (EPR), lo que se utilizará como mecanismo de targeting pasivo. Las LUVs se prepararon mediante hidratación de película delgada y fueron caracterizadas con dispersión dinámica de luz (DLS). La incorporación de HRP en las LUVs se consiguió mediante hidratación. Fueron caracterizadas mediante DLS, análisis de seguimiento de nanopartículas (NTA) y microscopía electrónica de transmisión (TEM). Finalmente, se realizaron experimentos celulares preliminares para evaluar la biocompatibilidad de las LUVs cargadas con HRP en cultivos *in vitro* de células de cáncer de melanoma SK-Mel-103. Para evaluar la viabilidad celular se llevó a cabo el ensayo WST-1. Los LUVs cargados demostraron ser biocompatibles, lo que abre la posibilidad de evaluar sus propiedades terapéuticas en futuros estudios. Este proyecto abre interesantes perspectivas para la aplicación de liposomas cargados con HRP en la investigación del cáncer.

Palabras clave: liposomas, LUVs, cáncer, nanomedicina, HRP, terapia enzima-profármaco, EPT

Autor: Marta Blázquez Ruiz
Tutor: Dr. Antoni Llopis Lorente
Co-tutor académico: Jordi Ventura Cobos
Co-tutor experimental: David Bastante Rodríguez

Valencia, abril de 2024

I would like to acknowledge and give my honest thanks to my supervisor Dr. Antoni Llopis and co-tutors Jordi Ventura and David Bastante, who helped me with dedication and kindness throughout all the project. Their support guided me these months, welcoming me into the laboratory and sharing their knowledge and expertise.

I am also grateful to Professor Ramón Martínez-Máñez, for hosting me in his labs in the Interuniversity Research Institute for Molecular Recognition and Technological Development (IDM) and Príncipe Felipe Research Center Foundation (CIPF). Working alongside experienced scientists in the field of nanomedicine has been a very valuable experience.

To my family, for their love and support, and for giving me the opportunity to study Biotechnology at the Polytechnic University of Valencia, and to my friends, for their companionship and positivity, making each day so enjoyable.

1. INTRODUCTION

1.1 Nanoparticles as drug delivery systems in cancer therapies

Nanotechnology is defined as the intentional engineering and manipulation of nanoparticles, particulate matter with a dimension in a size range of 1 nm to 100 nm. It is a relatively new scientific discipline that in the last two decades has gained increasing attention, with significant progress in the field of medicine, enhancing drug delivery systems (1).

Nanoparticle (NP)-based drug delivery systems offer improved stability and biocompatibility, precise targeting and the potential to innovate administration routes (2). As a result, this approach holds the potential to enhance biodistribution and prolong the life cycle of drugs, avoiding immunogenicity and reducing toxicity and side effects (3).

In the context of cancer treatment, where the need for effective therapies is urgent due to its profound global impact, nanotechnology holds immense promise. Cancer is responsible of 10 million people's death per year globally, remaining as one of the most common and lethal diseases in the world (1). The World Health Organization (WHO) estimates that by 2040 the number of new cancer cases per year will rise to 29.5 million, and the number of cancer-related deaths to 16.4 million (4).

One of the most used cancer treatment methods is chemotherapy. Unlike radiation therapy or surgery, chemotherapy relies on the administration of drugs. Although chemotherapy works through a number of mechanisms, its primary role involves the non-selective destruction of rapidly dividing cells, encompassing both tumor and healthy cells. This indiscriminate action results in severe side effects, including bone marrow suppression, hair loss, and gastrointestinal reactions. Henceforth, major efforts have been dedicated in research to the development of drugs that can more precisely target tumor cells, avoiding normal cells. Despite the new advancements in targeted therapy, we still face important problems such as drug resistance.

NP-based drug delivery systems for cancer treatment offer good pharmacokinetics, enhanced drug therapeutics, precise targeting of tumor cells and reduction of drug resistance and side effects; they can increase the half-life of drugs and stimulate their assembly into tumor tissues due to the size and surface characteristics of NPs and their ability of improving permeability and retention (2). Simultaneously, cytotoxicity in healthy cells is controlled and avoided through the targeting systems. For instance, PEGylated liposomes loaded with doxorubicin demonstrated a reduction in cardiotoxicity compared to the free form of the drug (5). Furthermore, NP-based drug delivery systems have demonstrated several advantages regarding multidrug resistance (MDR), as they are able to inhibit the functioning of certain mechanisms responsible for drug resistance, like efflux transporters on cell membranes (6). Currently, reports indicate that therapies utilizing NPs have the potential to overcome MDR in ovarian, breast and prostate cancer (2).

1.1.1 Types of NPs used for cancer treatment

Various forms of nanoparticles (NPs) are employed in cancer therapy. NPs utilized in drug delivery systems encompass organic and inorganic NPs (Figure 1). Within organic NPs, there are liposomes, polymer-based NPs, and dendrimers. Among polymer-based NPs, both coacervates and polymeric micelles are commonly used. Inorganic NPs include gold NPs, carbon nanotubes, silica NPs, magnetic NPs, and quantum dots. Moreover, exists a combination of both types in hybrid NPs, that incorporate lipid-polymer hybrid NPs, organic-inorganic hybrid NPs, and cell membrane-coated NPs (2).

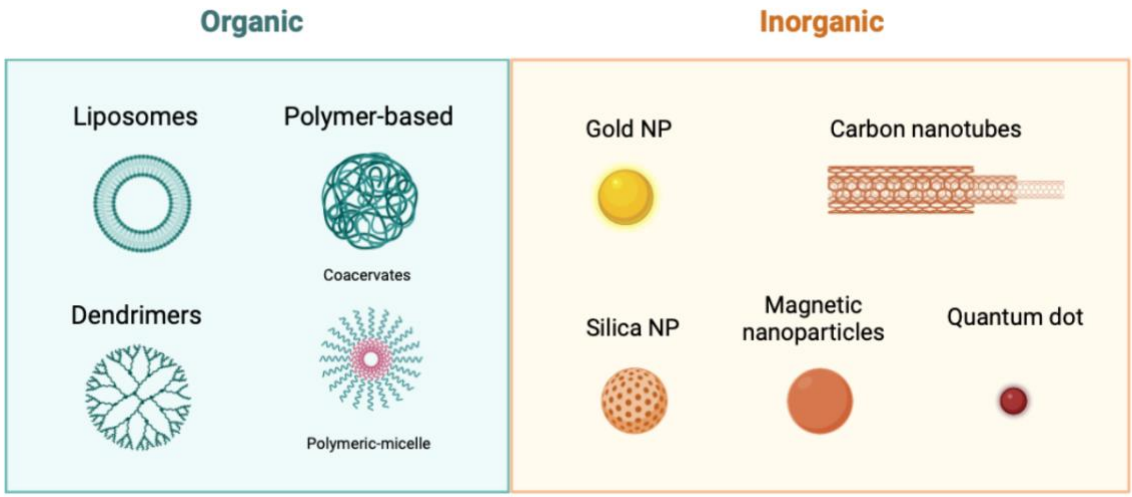

Figure 1. Types of organic and inorganic nanoparticles employed in cancer therapies.

1.1.2 Targeting of cancer cells: enhanced permeability and retention (EPR) effect

Directing nanoparticles (NPs) to cancer cells can be accomplished through passive or active targeting. Targeting of NPs improves the effectiveness of therapeutic interventions and minimize the potential for systemic toxicity. Passive targeting relies primarily on the enhanced permeability and retention (EPR) effect, while active targeting involves the interaction between specific ligands and receptors (7).

Passive targeting utilizes the distinctive characteristics of both tumor and normal tissues. The heightened proliferation of cancer cells leads to the formation of new blood vessels, resulting in larger pores in the vascular walls of tumor vessels compared to normal vessels. This defective angiogenesis enables NPs to escape from blood vessels supplying the tumor and accumulate within the tumor tissue (Figure 2). Simultaneously, the inadequate lymphatic drainage associated with cancer contributes to the prolonged retention of NPs, enabling the nanocarriers to release their contents into the tumor cells. These processes collectively give rise to the EPR effect, a key factor in passive targeting. The EPR effect's efficacy is influenced by the size of NPs, with numerous studies indicating that smaller NPs exhibit enhanced penetrability without leakage into normal

vessels. Likewise, larger particles are more prone to clearance by the immune system (8).

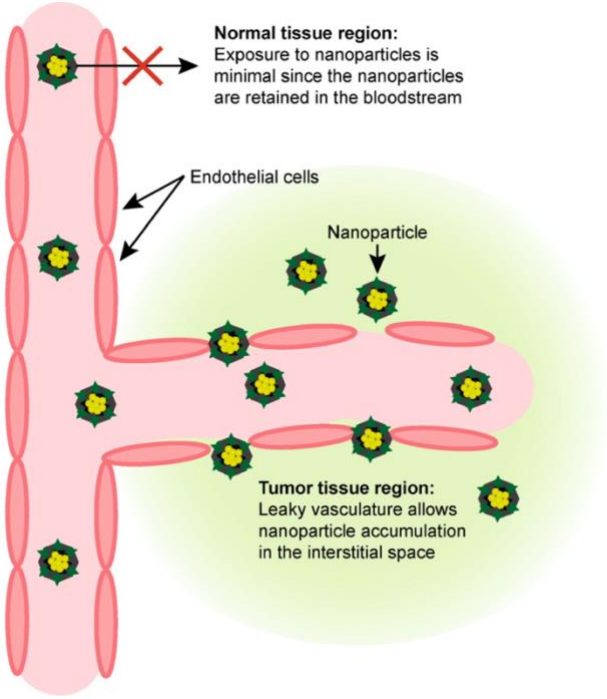

Figure 2. Representation of enhanced permeability and retention of nanoparticles in tumors. Contrast between normal tissue and tumor tissue with leaky vasculature that allows nanoparticle accumulation (8).

1.2 Liposomes

Liposomes are micro/nano-sized spherical vesicles composed of an aqueous core surrounded by one or more phospholipid bilayer shells (9). They present important characteristics such as biocompatibility, biodegradability, and low immunogenicity. Moreover, they have also proved to enhance drug solubility and controlled distribution, as well as their capacity for surface modifications for targeted, prolonged, and sustained release (10).

Due to these significant advantages, liposomes have been widely employed in nanomedicine and biomedical applications such as immunoassays, clinical diagnostics and tissue engineering. Particularly important is the role of liposomes in drug-delivery applications, enhancing the performance of encapsulated drugs and leading to a reduction in side effects and toxicity (9).

The size of liposomes can vary, spanning from 1 nm to several microns. For injectable clinical applications, all liposome formulations are within the submicron ultra-filterable range, measuring less than 200 nm in size (10). Regarding to the lamellarity of the underlying vesicle structures, liposomes can be classified into small unilamellar vesicles (<100 nm or SUVs), large unilamellar vesicles (100–1000 nm or LUVs), and giant unilamellar vesicles (>1 μm or GUVs) (Figure 3). Alternatively, multilamellar vesicles (MLVs) exhibit an onion-like structure consisting of concentric bilayer surfaces.

Unilamellar vesicles demonstrate a faster drug-release rate compared to MLVs, which, conversely, boast a larger entrapped volume (11).

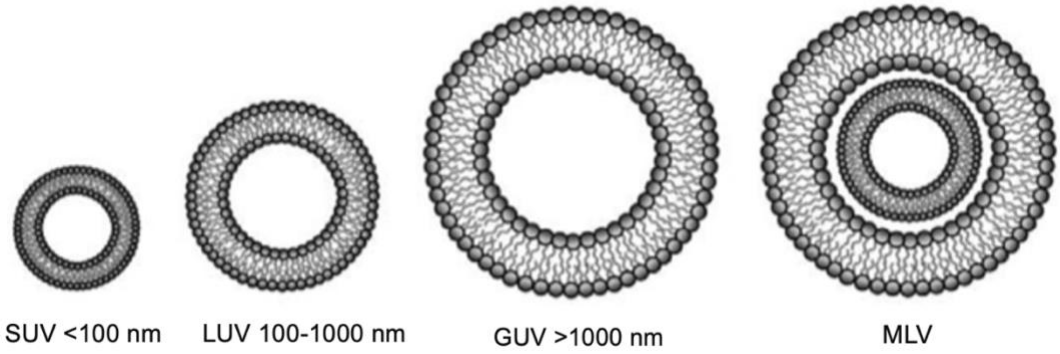

Figure 3. Schematic representation of the main classification of liposomes (12).

1.2.1 Liposomes in cancer therapies

In the context of cancer therapy, liposomes provide a robust platform for the *in vivo* delivery of various anti-tumor drugs. For instance, pegylated liposomal doxorubicin (Doxil) (Figure 4) was the first liposome with anti-cancer effects approved by the FDA. It consists of a formulation of doxorubicin in poly(ethylene glycol)-coated liposomes that provide prolonged circulation time and a unique toxicity profile.

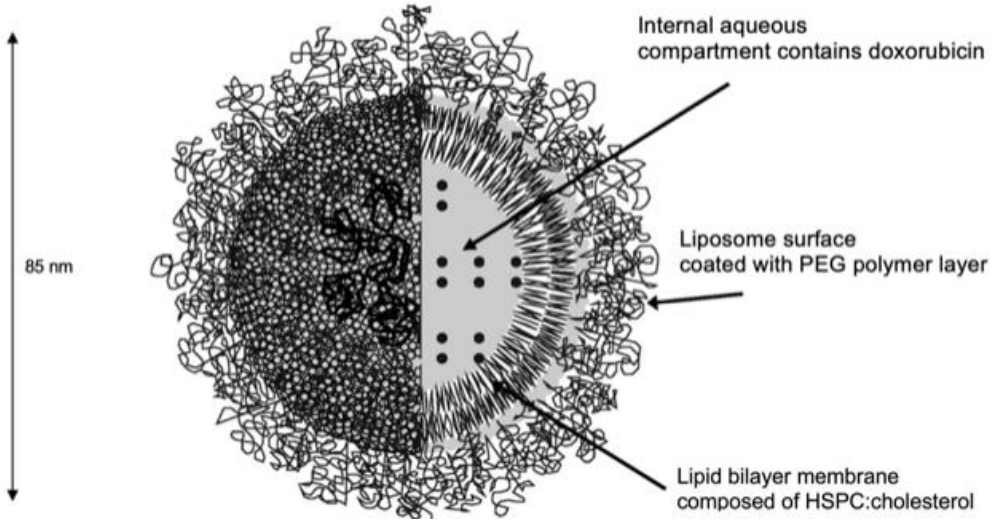

Figure 4. Cross-sectional view of a Doxil liposome. HSPC = hydrogenated soy phosphatidylcholine (13).

Doxil is likely among the most effective agents for AIDS-related Kaposi's sarcoma and plays a clear role in the treatment of recurrent ovarian cancer, which allow us to understand the importance of this type of therapies for cancer treatment (14). In breast

cancer treatments, several paclitaxel liposomes have also demonstrated heightened anti-tumor efficacy and enhanced bioavailability compared to free paclitaxel (15).

The dimensions of liposome nanoformulations (preferably ranging between 50 and 500 nm for biomedical applications) significantly impact their drug delivery process. Liposomes with diameters between 100–150 nm promote cell uptake and possess the ability to traverse the capillaries of blood vessels within diseased tissues and access tumor environments through fenestrated vessels. Additionally, liposomes measuring 50–100 nm or less in size can evade clearance by the immune system's phagocytosis, leading to extended blood circulation times (9).

1.3 Enzyme therapies

Enzymes have risen in the last decades as promising therapeutic tools for a wide range of pathologies. Treatments based on the catalytic activity of enzymes present several advantages compared to established therapeutic approaches, thanks to their affinity and specificity properties (16). Disorders such as cancer, cardiovascular diseases, fibrosis or metabolic deficiencies are already being treated by the 39 US Food and Drug Administration (FDA)-approved enzymes for clinical applications (17). In this growing field, research is still ongoing to solve health problems such as COVID-19. Currently, many angiotensin-converting enzyme 2 (ACE2) derivatives are being formulated as potential substitutes for traditional inhibitors targeting SARS-CoV-2 (18).

However, enzymes present some challenges, such as short *in vivo* half-life, lack of targeted action and patient immune system reactions against the enzyme. In order to become widely used drugs, enzyme therapies must overcome these drawbacks. Some of the most noteworthy techniques addressed to date belong to the nanotechnology field, such as enzyme encapsulation for drug delivery systems (19).

1.4 Horseradish peroxidase (HRP)

Horseradish peroxidase (HRP) is a class III member of the non-animal peroxidases and is commonly isolated from the horseradish plant *Armoracia rusticana* (20). Horseradish peroxidase has been the subject of scientific research for decades (21). HRP C is a monomeric glycoprotein primarily composed of α-helices, with a molecular weight of 44 kDa. Additionally, HRP contains four disulfide bonds and two calcium ions, both crucial for maintaining the enzyme's structural integrity. Figure 5 illustrates the overall configuration of HRP isoenzyme C1A, along with the arrangement of its active site, a feature common to all plant peroxidases.

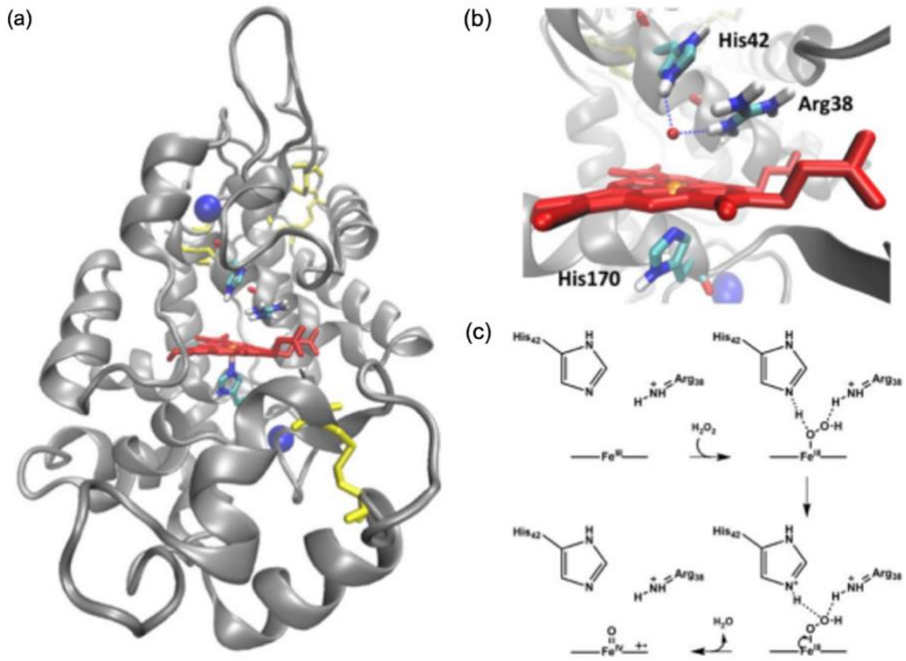

Figure 5. Crystal structure of HRP and the process of hydrogen peroxide reduction. (a) Overall three-dimensional structure of HRP C1A. The polypeptide chain is represented as a grey cartoon, while the heme cofactor, disulfide bonds, and specific amino acids are red, yellow, and multi-colored sticks, respectively. The presence of two calcium ions is indicated by blue spheres. (b) Detailed view of the active site of HRP C1A, with the heme cofactor shown as red sticks and the iron center represented as an orange sphere. The amino acids Arg38, His42, and His170 are blue sticks. (c) Mechanism for the reduction of hydrogen peroxide by heme peroxidases, leading to the formation of Compound I (22).

Figure 5b provides a close-up view of the active site, highlighting the cofactor and three specific amino acids. These amino acids are recognized as highly conserved and indispensable for the optimal activity of heme peroxidases. During catalysis, the distal amino acids Arg28 and His42 facilitate the effective cleavage of bound peroxide molecules by abstracting and donating protons, while also stabilizing leaving groups, as shown in figure 5c. (22)

1.4.1 Mechanism of cytotoxicity with IAA

Enzymes are very useful tools in biocatalysis, as reactions can be carried out under simple conditions concerning temperature, pressure and solvent. A major field that uses HRP is oxidative dehydrogenation of different substrates, such ferulic acid or tyrosine derivatives. This reaction generates an oxidative stress ambient that can be truly valuable for biomedicine applications. Particularly, the combination of HRP with indole-3-acetic acid (IAA) has shown promising results (23). Indole-3-acetic acid (IAA) is the predominant form of the plant growth hormone auxin in higher plants, playing a crucial role in regulating plant cell division, elongation, and differentiation. Recently, studies have indicated that the combination of IAA and horseradish peroxidase (HRP) exhibits cytotoxic effects on mammalian cells.

IAA can be used as a non-toxic prodrug as it is well tolerated by humans. The reaction between IAA and HRP proceeds through a complex mechanism that remains to be elucidated. HRP catalizes the oxidation of IAA and produce free radicals such as indolyl, skatolyl, and peroxyl, inducing cellular oxidative stress and leading to cell death (24).

1.4.2 Anticancer potential of HRP/IAA

Enzyme-prodrug therapy (EPT) seeks to apply enzymes that are not toxic in themselves but can catalyze activation of prodrugs, which are also non-toxic, to produce a toxic drug at targeted locations. In the past few years, the combination of IAA and HRP has been proposed as a novel cancer therapy.

The signaling pathways in apoptosis are potential targets for cancer therapy. Two main apoptotic pathways have been identified in mammalian cells (Figure 6) (25). Death receptors such as Fas (also known as CD95) and tumor necrosis factor receptor 1 (TNFR1) activate caspase-8, whereas caspase-9 is activated via the mitochondrial pathway. Activated caspase-8 or caspase-9 can cleave and activate executive caspases, like caspase-3, which mediates the cleavage of a DNA repair enzyme, resulting in the morphological nuclear changes associated with apoptosis.

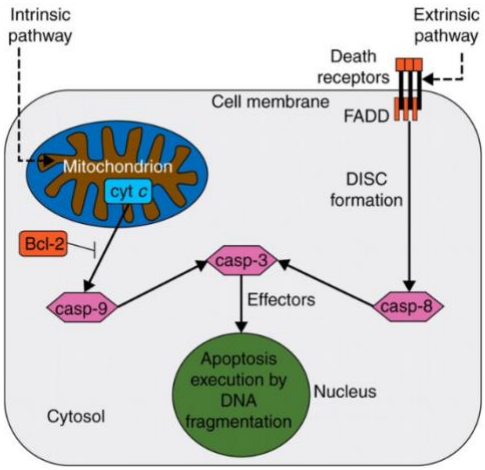

Figure 6. Two major pathways of apoptosis. In the left side, the mitochondrial way which involves mitochondrial dysfunction, release of cytochrom c and activation of caspase-9. In the right side, the death receptor pathway initiated by binding of death ligands to death receptors and activation of caspase-8 (25).

The oxidative stress caused by the reactive oxygen species (ROS) generated by HRP/IAA combination results in DNA base modifications. These include single- and double-strand breaks and the formation of apurinic/apyrimidinic lesions, many of which are toxic and/or mutagenic (26). Both death receptor-mediated and mitochondrial apoptotic pathways are activated through the cytotoxic species, reducing the cell viability of carcinoma cells. Neither the prodrug IAA nor the enzyme HRP C1A alone demonstrates cytotoxicity, as this process has reportedly been shown to be tolerable for humans (20).

Furthermore, HRP has significant characteristics that make it advantageous for medical applications. These include high stability at 37 °C, non-toxic nature, high catalytic activity at neutral pH, and ease of conjugation to antibodies and polymers (20).

Compelling investigations have been conducted in this field, offering promising results to overcome current clinical constraints of cancer treatment. It is the case of an interesting work developed about enzyme-functionalized gold nanoparticles designed and evaluated to efficiently carry out enzyme prodrug therapy (EPT) in triple negative breast cancer (TNBC) cells. HRP is incorporated on gold nanoconjugates (HRP-AuNCs) and treated with IAA, releasing toxic oxidative species. The nanoplatform proved to be effective and breast cancer cells viability was reduced below 5% (27).

Exciting results like those motivate this work, as there have been no reports on the use of lipidic nanoparticle-HRP systems for EPT applications.

2. OBJECTIVES

The main aim of this work is to develop and evaluate large unilamellar vesicles (LUVs) encapsulating the enzyme horseradish peroxidase (HRP), as a novel nano-bio-platform to perform enzyme prodrug therapy (EPT) in cancer cells (Figure 7). It is expected to verify the effective assembly of LUVs with the proper size and monodisperse characteristics, obtain effective internalization of HRP into LUVs, ensure their stability and biocompatibility and achieve enhanced drug efficacy.

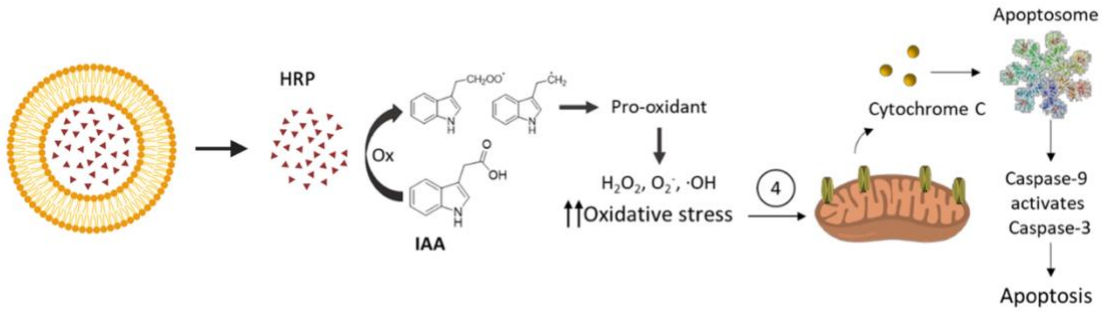

Figure 7. Representation of HRP liberation by passive diffusion and catalytic activity of the enzyme which produces a significant transformation of IAA into toxic radicals.HRP transforms IAA into indolyl and peroxyl radicals that lead to ROS generation and subsequent cell death by activation of apoptosis (Adapted from ref. 27).

In order to achieve these objectives, the following stages are followed:

1. Preparation of LUVs using the thin-film hydration method.
2. Purification and characterization of sodium fluorescein-loaded LUVs.
3. Purification and characterization of HRP-loaded LUVs.
4. Cellular studies to evaluate biocompatibility in SK-Mel-103 human melanoma cancer cells.

Nanotechnology possesses the ability to improve pharmacological profile of a drug increasing its efficacy while decreasing side effects. This project aims to address the underexplored domain of lipidic nanoparticle-HRP systems for enzyme-prodrug therapy (EPT) in cancer treatment.

3. MATERIALS

3.1 Materials

Cholesterol (C8667, Sigma Aldrich), 1, 2-dioleoyl-sn-glycero-3-phosphocholine (DOPC) (850375P, Avanti Polar Lipids), Methanol (439193, Sigma Aldrich), Chloroform (650498, Sigma Aldrich), Horseradish peroxidase (HRP) (SRE0082, Sigma Aldrich), Phosphate-Buffered Saline (PBS), Fluorescein sodium salt (F6377, Sigma Aldrich), Triton (X-100, Sigma Aldrich), Sepharose 4B (4B200, Sigma Aldrich), Sephadex G-50 (G5080, Sigma Aldrich), Centrifugal Filter Unit (UFC9010, Amicon Ultra Filters, Sigma Aldrich) PierceTM BCA Protein Assay Kit (Thermo Fisher Scientific, USA), 2,2'-Azino-bis(3-Ethylbenzthiazoline-6-Sulfonic Acid) (ABTS) (A1888, Sigma Aldrich) and Hydrogene Peroxide (H1009, Sigma Aldrich).

3.2 Equipment

V-650 UV-VIS Double-Beam Spectrophotometer (Jasko, Japan), Mini extruder (Avanti Polar Lipids, USA), Fluorometer FP-8050 Series (Jasko, Japan), Analyzer-ZetaSizer Nano ZS (Malvern Instruments Ltd, United Kingdom) Wallac spectrophotometer Victor2TM (PerkinElmer life science, USA) NanoSight (Malvern Instruments Ltd, United Kingdom), transmission electron microscope (JEOL TEM-1010 Electron microscope working at 100 kV), rotary evaporator and vacuum pump.

4. METHODS

4.1 Synthesis of large unilamellar vesicles (LUVs) using the thin-film hydration method

100 μL of DOPC and 21 μL of cholesterol (for 10 mg of lipids) are mixed in a 70:30 molar ratio and dissolved in a 1:1 solution of methanol and chloroform. This vial is placed in a rotary evaporator for 40 minutes at 40 °C and 440 mbar, which facilitates the evaporation of the solvent and the formation of a lipid film. To ensure complete drying, it is placed for at least 1 hour in a vacuum pump. Vesicle formation is achieved by hydration of the film using 1X PBS, leaving the vial in the rotary evaporator without pressure for 30 min, at 40°C. Next, an extrusion process (Avanti Mini Extruder) is carried out to ensure a monodisperse sample, using a 100 nm filter and repeating it at least 11 times. First, the extruder parts are pre-wetted with 1X PBS. Once the dead volume is thus reduced, the sample is loaded into one of the gas-tight syringes that the kit provides and placed at one end of the mini extruder. On the other side, the empty syringe is placed, which will be automatically filled when the lipid is extruded through the membrane. The process is repeated at least 11 times, and after the final extrusion, the sample will be collected from the opposite syringe to the original one to reduce the chances of contamination with

particles of external material. Finally, the extruded lipid solution is injected into a new vial and analyzed using dynamic light scattering (DLS).

4.2 Sodium fluorescein (SF)-loaded LUVs

The same procedure explained above was followed in order to obtain the dye-loaded liposomes. To encapsulate the dye, LUVs were hydrated with 80 mM SF in 1X PBS. 80mM SF was made from fluorescein powder. In this case, NaCl concentration of PBS was reduced in -80 mM in order to maintain the osmotic pressure. After completing the same previous protocol of extrusion, an exclusion chromatography was performed to purify LUVs. A size exclusion column with G-50 Sephadex was used, pre-wetting it in first place with 1X PBS. 14 fractions of 1 mL were collected starting 30 seconds after the introduction of the sample in the column, and analyzed with DLS.

4.2.1 Disruption of SF-loaded LUVs with Triton X-100

Firstly, a blank solution (PBS) was measured with the fluorometer, followed by the measurement of the 100x diluted dyed liposome solution in the same buffer. Fluorescein absorbs at 494 nm, so the measurements were taken between 500-700 nm. After that, LUVs were disrupted by incubating the sample with 10 μL of Triton X-100 2% solution for one minute, and then measured again at the same conditions.

4.3 Horseradish peroxidase (HRP)-loaded LUVs

The enzyme-loaded liposomes were produced using the same procedure by thin-film hydration explained previously. The hydration buffer was prepared by mixing 10 mg of solid HRP with 1 mL of PBS. After the extrusion as previously, liposomes were purified by size exclusion chromatography. In this case, a column with Sepharose 4B was used to get rid of the not-loaded enzyme. Two batches of LUVs encapsulating HRP were prepared within a time difference of two months, in order to prove the robustness of the technique and to obtain freshly prepared LUVs to continue with the experiments. After purification, 24 fractions of 0.5 mL were collected from the column in the case of the first batch, and analyzed using the dynamic light scattering (DLS) technique, nanoparticle tracking analysis (NTA) and transmission electron microscopy (TEM). In the case of the second batch, 12 fractions of 1 mL were collected and analyzed by DLS.

4.3.1 Enzyme quantification with BCA protein assay

The protein content of the nanoparticles was determined using the BCA protein assay. Two assays were performed, one for each batch of LUVs encapsulating HRP. In order to obtain a calibration curve, HRP was measured at four different concentrations in the range of 50 μg/mL and 500 μg/mL for the first batch, and in the range of 25 μg/mL to 300 μg/mL for the second batch.

With the aim of obtaining these measurements, HRP solution (1 mg/mL) was prepared and the PierceTM BCA Protein Assay Kit was used. The working reagent was attained

by mixing 50 parts of BCA Reagent A with 1 part of BCA Reagent B. HRP solution was mixed with reagents and incubated at 60 °C for 30 minutes in a tube shaker at 500 rpm. The curve was plotted from the absorbances measured at 562 nm in the spectrophotometer. The fraction number 9 (milliliter 4.5) of LUVs collected was mixed with the kit reagents and the same procedure of incubation was followed. Likewise, fraction 4 (milliliter 4) from the second batch of LUVs prepared had the same protocol. The amount of enzyme in the nanoparticles was quantified using the equation obtained with the calibration curves and the signal of the sample assays.

4.3.2 Enzyme activity assay

The activity of LUVs encapsulating horseradish peroxidase was determined through an enzyme activity assay. 2,2'-Azino-bis(3-Ethylbenzthiazoline-6-Sulfonic Acid) (ABTS) was used as substrate. In the presence of HRP, hydrogen peroxide (H_2O_2) reacts with ABTS and gives a green colored product (ABTS+), which can be measured by a spectrophotometer at 418 nm.

Firstly, 200 μL of 1x PBS were transferred to a quartz cuvette and used as baseline. For the blank, 193.2 μL of ABTS (1mg/mL), 16.6 μL of H_2O_2 (10 mM) and 4 μL of 1x PBS buffer were added to the quartz cuvette. Measures at 418 nm were carried out for 4 min every 5 seconds. Then, 193.2 μL of ABTS (1mg/ml), 16.6 μL of H_2O_2 (10 mM) and 4 μL of HRP-loaded LUVs (96.25 μg/mL), were added to the quartz cuvette and absorbance was measured at the same parameters as a function of time.

HRP-loaded LUVs with dimethyl sulfoxide (DMSO) were prepared in order to disrupt LUVs and test if enzyme activity increased after the enzyme release. 10 μL of HRP-loaded LUVs (96.25 μg/mL) were mixed with 10 μL of DMSO and kept for 30 minutes at 37 °C in a tube shaker at 500 rpm. For the spectrophotometer measure, 193.2 μL of ABTS (1mg/mL), 16.6 μL of H_2O_2 (10 mM) and 8 μL of the disrupted LUVs were added to the quartz cuvette and measured as explained previously.

An analysis of the enzymatic activity of free HRP over a period of time of 1 month was also conducted in order to evaluate its stability and reliability. Free HRP 1 mg/mL was prepared and kept at 4 °C between measurements. Same procedure as previously was followed, adding 193.2 μL of ABTS (1mg/mL), 16.6 μL of H_2O_2 (10 mM) and 4 μL of free HRP (1 mg/mL) to the quartz cuvette and measuring absorbance at 418 nm. Measures were taken in days 1, 14 and 21 after preparation.

4.4 LUVs characterization

Characterization of LUVs was done using three methods: dynamic light scattering (DLS) technique, nanoparticle tracking analysis (NTA) technique and transmission electron microscopy (TEM).

By DLS technique we measured the polydispersity index (PDI), z-average and zeta potential (ZP). The measures were performed through a Zetasizer Nano S from Malvern

Instruments Ltd. 200 μL of sample were introduced in a quartz cuvette ZEN0118 from Hellma Analytics and measured. The utilized SOP was adapted for lipid compounds: the refractive index (RI) was 1.456 and absorption was 0.1.

For NTA technique, measures were performed using a Nanosight NS300 instrument from Malvern Panalytical. A 1:3000 dilution in MiliQ water was obtained from LUVs containing peroxidase (96.25 μg/mL) and 1 mL was injected into the Nanosight port with a disposable syringe. The detect threshold was set to 11 and measures were taken for 5 minutes in time ranges of 1 minute and 20 seconds.

In order to observe LUVs by TEM, 10 μL of sample were placed on parafilm, with a grid on top so that the liposomes stuck to the membrane. After 15 minutes, the grid was removed with the liposomes already attached, and it was floated on 10 μL of 2% uranyl acetate. Five minutes later, a filter paper was used to dry the border of the grid and was left to air dry for two hours. Finally, it was observed at TEM.

4.5 Concentration of LUVs

LUVs were concentrated using a Microcon-10kDa centrifuge filtration unit with Ultracel-10 membrane from Sigma Aldrich. The column was filled with 0.5 mL of LUVs and centrifuged twice for 10 minutes at 7000 rpm. Then, the retained fraction in the column was collected and diluted 3000 times in MiliQ water in order to measure its concentration in the Nanosight. It was injected through a disposable syringe in the port of the Nanosight and same conditions as previously were set.

4.6 Cell experiment

4.6.1 Culture conditions

For the cell assay, SK-Mel-103 (human melanoma cancer cells) were utilized. Cells were purchased from ATCC and cultured in Dulbecco's Modified Eagle's Medium (DMEM) supplemented with 10% fetal bovine serum (FBS). Incubation of the cells was carried out at 37°C with 5% CO2 and 95% air. Cells were washed with phosphate buffered saline (PBS) and detached with Trypsin-EDTA 0,05% before transferring to new vessels. Cell culture procedures were performed under sterile conditions within a laminar flow cabinet.

4.6.2 Cell viability assay

4.6.2.1 Biocompatibility studies with HRP-LUVs

The biocompatibility of HRP-LUVs was assessed in SK-Mel-103 cells. The cytotoxic effect was evaluated by WST-1 assay. SK-Mel-103 cells were seeded into 96-well plates at a density of 5000 cells per well, after being counted through Neubauer chamber analysis. Following 24 hours of incubation, the cells were exposed to varying concentrations of HRP-loaded LUVs (10 μg/mL, 50 μg/mL), for another 24 hours. After

that incubation time, WST-1 (10 μL per well) was added and incubated for 1 hour. The absorbance was recorded at 450 nm at Wallac Victor2TM spectrophotometer (PerkinElmer).

4.6.2.2 HRP-loaded LUVs for EPT in Melanoma Cancer Cells

Enzyme-prodrug therapy, carried out by HRP-loaded LUVs in combination with IAA, was evaluated in SK-Mel-103 cells (5000 cells/well). The cells were seeded on 96-well plates one day before treatment. The cytotoxic effect of EPT was assessed after treatment with HRP-loaded LUVs or free HRP in the absence or presence of IAA at a concentration of 1 mM for 24 hours. HRP-loaded LUVs were used at varying concentrations of HRP (1 μg/mL, 2 μg/mL, 5 μg/mL, 10 μg/mL), in combination with IAA 1 mM. Likewise, free HRP was used at the same range (1 μg/mL, 2 μg/mL, 5 μg/mL, 10 μg/mL) with IAA 1 mM. These concentrations were chosen based in the literature, which indicated that concentrations at or above this threshold consistently yielded robust and reliable results (28) (29) (30) (31).

Untreated cells and single-agent treatment, ie, HRP (10 μg/mL, 50 μg/mL), HRP-loaded LUVs (10 μg/mL, 50 μg/mL) and IAA (1 mM, 5 mM), were used as controls. After 24 hours of incubation, WST-1 (10 μL/ well) was added and incubated for 1 h. The absorbance was recorded at 450 nm at Wallace 1420 workstation.

5. RESULTS AND DISCUSSION

5.1 Development of HRP-loaded LUVs

Liposomes are characterized by easily controllable properties such as lipid composition, size, structure and surface charge. The primary objectives of a technique for creating liposome nanoformulations are achieving the generation of monodisperse particles, with the desired degree of lamellarity, effective incorporation of drugs, and sustained colloidal stability of the final products.

LUVs were obtained by the thin-film hydration method. This technique was chosen for being a robust and simple approach which has already being employed to encapsulate a large variety of lipophilic drug molecules such as Paclitaxel (PTX) or Docetaxel (DCX) as well as a variety of hydrophilic ingredients, such as proteins or small interfering RNA (siRNA) (9). Two batches of HRP loaded liposomes were prepared, in order to assure the reproducibility of the experiments.

5.1.1 Preparation of liposomes

The first objective of this work was to verify the effective assembly of LUVs with the proper size and monodisperse characteristics required. In order to accomplish that, LUVs were created following the thin-film hydration method.

A thin-film lipid layer was created by dissolving the lipids DOPC and cholesterol with a 70:30 molar ratio in a chloroform/methanol solution (1:1) within a round-bottom vial. Cholesterol molecules cause the membrane to become more stable, leading to a decrease in permeability to water and other molecules (32).

After removing the solvent, a hydration process was carried out by the addition of an aqueous buffer (1X PBS), where the thin lipid film swells to produce round close liposomes. Subsequently, the lipid vesicles were extruded 11 times through a 100 nm filter using the Mini Extruder. This pore size was selected because liposomes ranging from 100 to 150 nm in diameter enhance cellular uptake and possess the capability to traverse capillaries in the blood vessels within afflicted tissues and penetrate tumor environments through fenestrated vessels (11). After the extrusion, LUVs were analyzed with dynamic light scattering (DLS). The whole preparation process is represented in Figure 8.

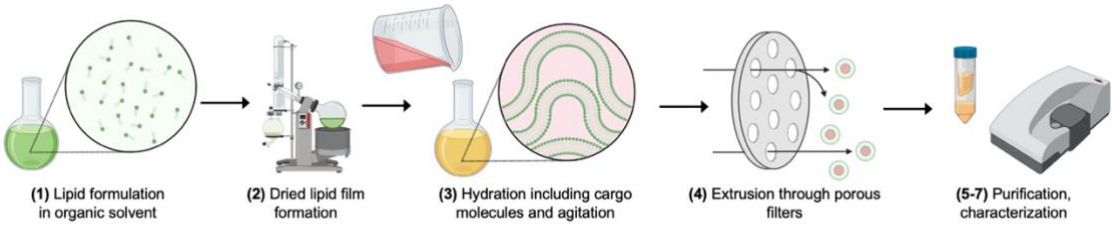

Figure 8. Steps followed for LUVs preparation by thin-film hydration method.

5.1.1.1 Characterization with DLS

DLS results indicated that the assembly and extrusion of LUVs was successfully performed. The obtained polydispersity index (PDI) was 0,09 ± 0,017, z-average size 145 ± 1,231 nm and zeta potential (ZP) -6 mV ± 0.776.

PDI is a parameter provided by DLS that indicates the heterogeneity of a sample based on size. Polydispersity can occur due to size distribution in a sample or agglomeration or aggregation of the sample during isolation or analysis. A PDI of 0.3 and below is considered to be acceptable and indicates a homogenous population of lipidic vesicles (33). On the other hand, z-average is the weighted average hydrodynamic size of the particle ensemble, and it is required to be below 200 nm for passive targeting tumor tissues via EPR (34). Zeta potential (ZP) is a physical property that controls electrostatic interactions in particle dispersions and is essential in understanding the stability of colloidal dispersions (35). Furthermore, ZP parameter gives information about the stability circulation time, protein interactions, permeability and biocompatibility of the

nanoparticles. Some studies revealed that particles with a slight negative zeta potential and a vesicle size of 150 nm are prone to accumulate in tumors (36).

5.1.2 Preparation of SF-loaded liposomes

In order to check the cargo-loading into LUVs, we encapsulated sodium fluorescein (80 mM). It is an effective approach to ensure the LUVs encapsulation as it results in measurable fluorescence after LUVs disruption. Liposomes were prepared by thin-film hydration method following the same protocol as in the previous experiment, and hydrated with fluorescein solution. Extrusion was carried out using 100 nm filters and 11 passes through the extruder. The extruded LUVs were analyzed by DLS, obtaining a PDI value of 0,147 ± 0,016 and z-average of 152.9 ± 1,13 nm. We can conclude from these results that LUVs were successfully obtained by extrusion.

Once we confirmed the extrusion was correct with DLS, we performed a purification to remove free dye. Size exclusion chromatography (SEC) was the chosen method, and the sample was placed into a Sephadex G-50 column. SEC separates solutes of different size, based upon the size exclusion effect of the porous gel packed in the column. Big molecules are the first to elute, as small molecules get inside the pores and have a longest retention time (37). Consequently, LUVs will elute firstly as the free fluoresceine dye has a smaller size. In figure 9, we can clearly differentiate where the free dye is in the column, through the strong orange color. Moreover, we can distinguish another lighter orange fraction in the column, closer to the bottom, which corresponds to the SF-loaded LUVs.

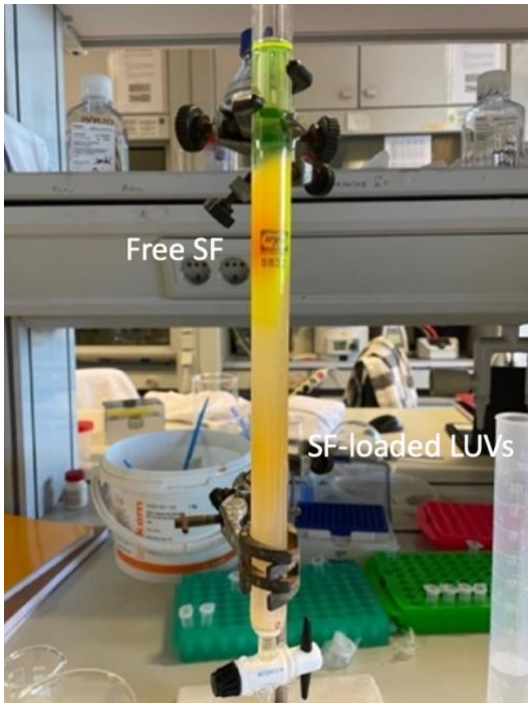

Figure 9. Size exclusion chromatography of sodium fluorescein loaded LUVs, by Sephadex G-50 column.

In order to equilibrate the column, it was pre-wetted before loading the sample using PBS buffer. After it, the sample was loaded with 400 μL of extruded LUVs and 14 fractions of 1 mL were collected. We begin to collect them when the colored sample was about to leave the column, obtaining the fractions showed in Figure 10.

Figure 10. 14 fractions of LUVs with fluorescein collected after purification with SEC.

5.1.2.1 Characterization with DLS

Fractions 4 and 10 were analyzed with DLS. Fraction 10 (milliliter 10) obtained a PDI of 0,127 ± 0,011 and a z-average of 149.8 ± 1,421 nm (Figure 11), whereas fraction 4 showed a PDI of 0.177 ± 0,021 and a z-average of 164.9 ± 1,274 nm. From these results we confirm that SEC does not influence the sample characteristics and is an effective purification method.

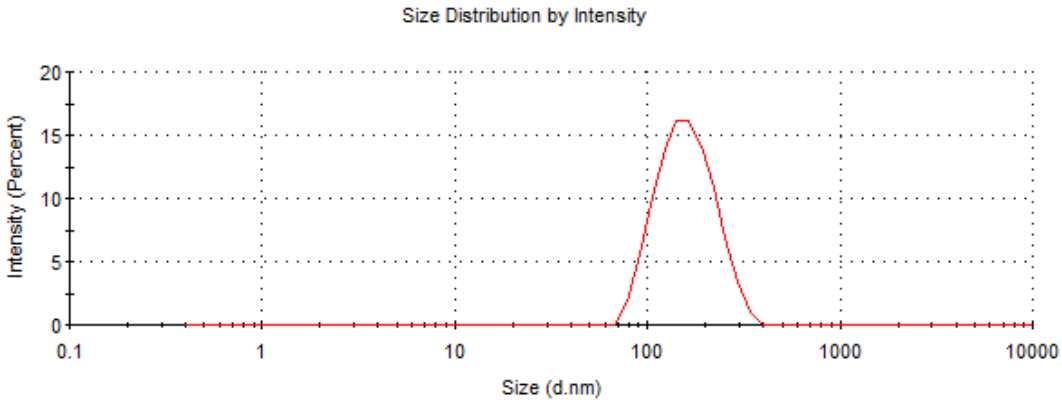

Figure 11. Size distribution by intensity of fraction 10 (milliliter 10) SF-loaded LUVs after SEC, measured with DLS.

5.1.2.2 LUVs disruption with Triton X-100

A release experiment was performed mixing Triton X-100 2% with the sample to disrupt LUVs and measure fluorescence intensity before and after the treatment. The aim of this experiment was to confirm that encapsulation had been successfully achieved, and that the release of the fluorescein was possible by disrupting the vesicle itself. Fluorescein

intensity of the sample buffer (PBS), the LUVs in that same sample buffer and LUVs after 1 minute incubation with the Triton solution, was measured in the fluorometer.

Fluorescence quenching is described as a decrease in fluorescence intensity due to one of several processes such as excited state reactions, energy transfer, complex formation, and collisional quenching (Lombardo & Kiselev, 2022a). This last concept means that the more concentrated our sample is, less fluorescein intensity will be detected, as it is quenched. SF inside LUVs is highly concentrated, so fluorescein intensity will be less than after its disruption, where the dye will be more diluted.

We can see in Figure 12 that the intensity of fluorescein increases approximately 10 times after the addition of Triton X-100. Therefore, we can conclude that the fluorescein was correctly encapsulated and that we are able to release it by the disruption of the liposome.

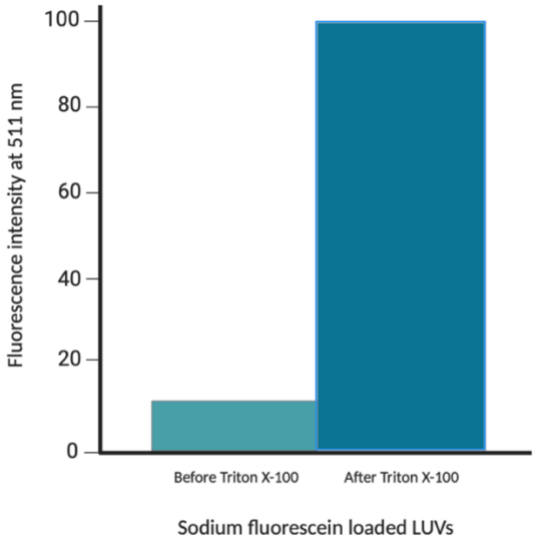

Figure 12. Fluorescence intensity measures before and after Triton X-100 treatment.

5.1.3 Preparation of HRP-loaded LUVs

After successfully encapsulating fluorescein into LUVs, the encapsulation of horseradish peroxidase was performed. LUVs were prepared with a thin-film hydration method as in the previous experiment. When the lipid film was formed, enzyme encapsulation was achieved by hydration of the film with enzyme solution in PBS (10 mg/mL), leaving the vial in the rotary evaporator without pressure for 30 min, at 40°C. HRP is hydrophilic, so it becomes entrapped within the aqueous interior of liposomes. Next, an extrusion process (Avanti Mini Extruder) was carried out to ensure a monodisperse sample, using a 100 nm filter and repeating it at least 11 times.

5.1.3.1 Characterization with DLS

Samples were analyzed with DLS before the purification, obtaining a PDI of 0,085 ± 0,022 and a z-average of 140.5 ± 1,631, which indicates that extrusion was successfully performed.
LUVs were purified by size exclusion chromatography using a column with Sepharose 4B to get rid of the non-encapsulated enzyme. First of all, the column was equilibrated with 5 mL of PBS. After extrusion, 900 μL of sample were loaded into the column.

Two batches of HRP loaded liposomes were prepared within a difference in time of two months, in order to ensure the robustness of the technique and to have freshly prepared LUVs to continue with the experiments. For the first batch, 24 fractions of 0.5 mL were collected from the Sepharose 4B column (Figure 13). For the second one, 12 fractions of 1 mL were collected. Fractions containing LUVs exhibit a cloudy white appearance, whereas free peroxidase appears orange in color. Due to their larger size, LUVs elute first from the Sepharose column. As we can see in Figure 13, fractions 8 and 9 (corresponding to milliliters 4 and 4.5) have this characteristic cloudy appearance, indicating the presence of LUVs. Similarly, this is observed in fractions 3 and 4 (equivalent to milliliters 3 and 4) of the second batch. The first batch was characterized by DLS, NTA and TEM, while the second batch was characterized just by DLS, as LUVs properties were already well established.

Figure 13. 24 fractions of HRP-loaded LUVs collected after purification with SEC.

From the first batch, fractions 6, 8, 9, 11, and 16 were analyzed using the dynamic light scattering (DLS) technique. Fraction 9, which is milliliter 4.5 expelled from the Sepharose column, was kept for future experiments as it had the most remarkable results (Figure 14). This fraction had a PDI of 0.065 ± 0.023, a z-average of 138.5 ± 1.725 and a ZP value of -9 mV ± 1,45.

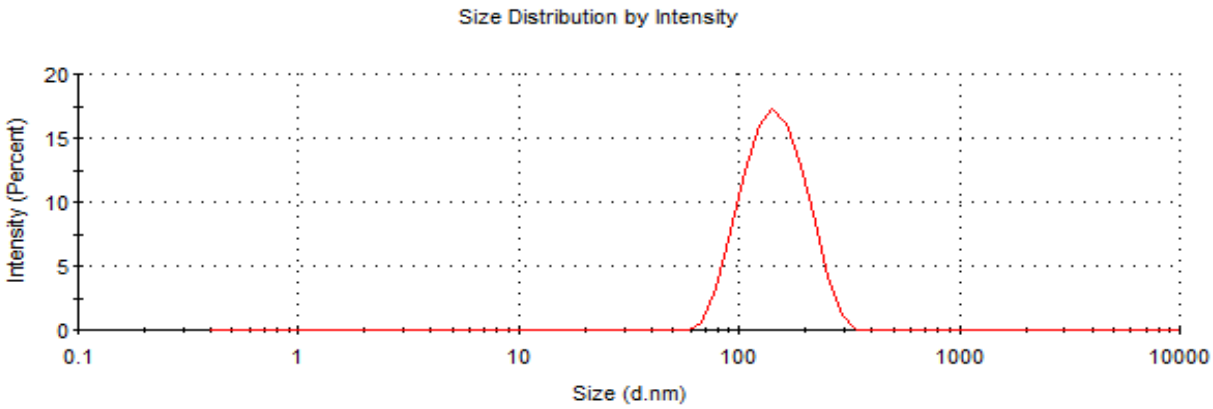

Figure 14. Size distribution by intensity of HRP-loaded LUVs from fraction 9 (milliliter 4.5 expelled from the Sepharose 4B column) from the first prepared batch, after SEC, measured with DLS.

From the second batch, fraction 4 (milliliter 4) was chosen for future experiments as it had the better results after its characterization by DLS (Figure 15). It obtained a PDI of 0.071 ± 0.011, a z-average of 141.5 ± 1.082 and a ZP value of -10 mV ± 1,53.

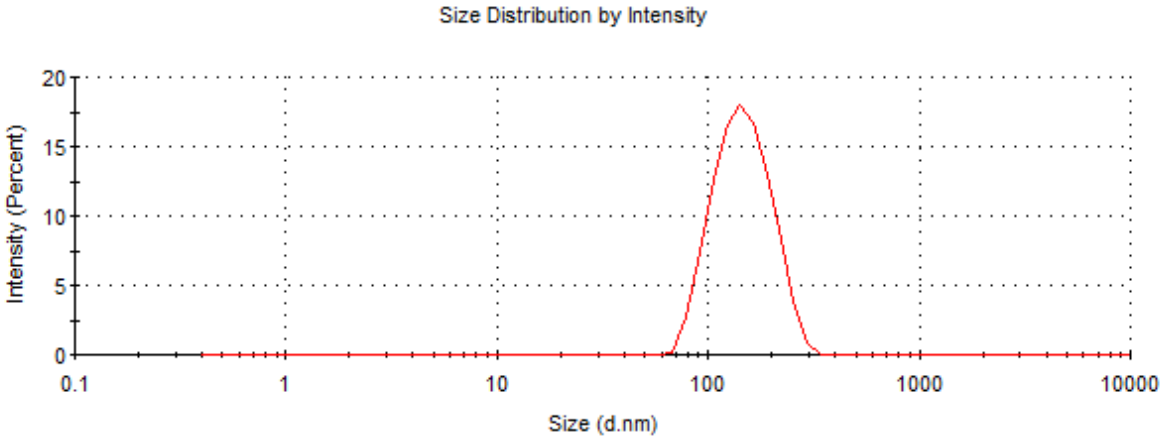

Figure 15. Size distribution by intensity of HRP-loaded LUVs from fraction 4(milliliter 4 expelled from the Sepharose 4B column) second prepared batch, after SEC, measured with DLS.

Through these results it can be concluded that LUVs were correctly assembled, as all parameters were in an appropriate range for stability and accumulation in tumor tissues (ZP), cell uptake and EPR effect (z-average). Monodisperse distribution was also assured as the PDI values were very commendable, being PDI values lower than 0.3 already considered acceptable.

5.1.3.1.1 Stability of HRP-loaded LUVs within time

Stability of HRP-loaded LUVs within time at different temperatures of storage was assessed by DLS. This study aimed to identify the most suitable storage conditions and

evaluate any degradation or changes in their properties, to ensure their functional integrity in diverse applications.

LUVs stored at 4 °C showed slight increases in size over 28 days, varying from 138.5 ± 1.725 nm in day 1 to 150.6 ± 0.996 nm in day 28 (Figure 16). However, these changes are minimal and do not raise significant concerns about LUVs stability. Furthermore, the PDI values range from 0.065 ± 0.015 on day 1 to 0.127 ± 0.018 on day 28. This suggests that while polydispersity increases over time due to some degradation of LUVs, the increase remains minimal and stays within the acceptable PDI range. Storing LUVs at 4 °C appears to maintain their structural integrity adequately, which aligns with established standards for lipid-based formulation preservation.

On the other hand, LUVs stored at ambient temperature (25 °C) experienced more noticeable increases in size over the same period (Figure 16). While these changes were not substantial, they suggest that refrigerated storage may be preferable to maintain consistent stability. However, it's important to highlight that storing LUVs at ambient temperature does not lead to significant harm, providing reassurance for situations where refrigeration might not be available. Similarly, PDI values indicate a slight increase in polydispersity, transitioning from 0.065 ± 0.015 on day 1 to 0.207 ± 0.036 on day 28. Nevertheless, they remain within the acceptable range for PDI.

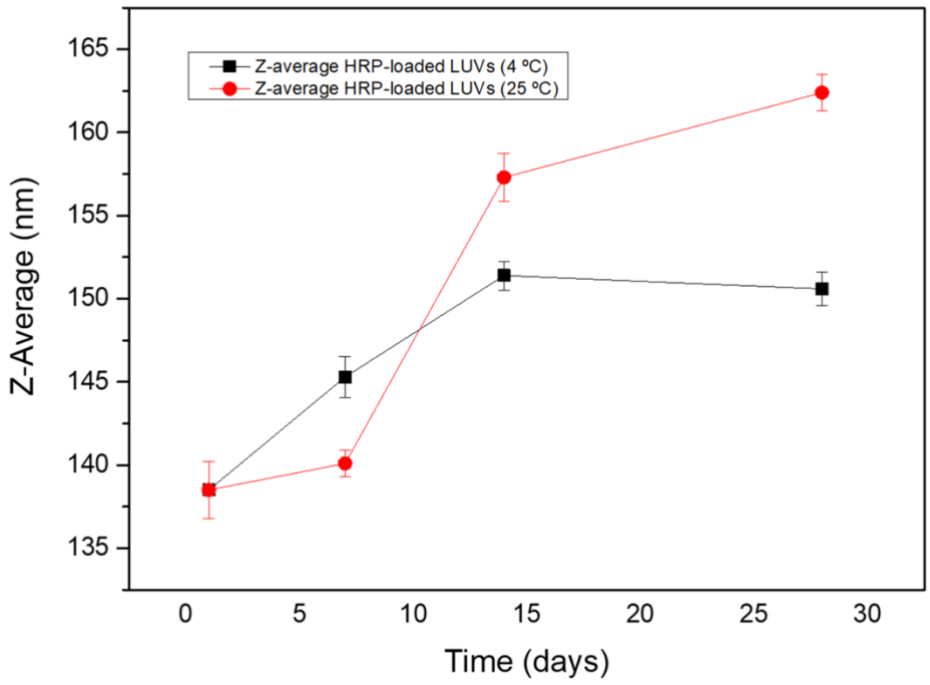

Figure 16. Stability of HRP-loaded LUVs (z-average) over time (days) stored at 4 °C and 25 ºC, measured with DLS.

Lastly, LUVs stored at -20 °C exhibited significant degradation. Z-average varied from around 138.5 ± 1.725 nm in day 1 to 1170 ± 6.52 nm in day 7. However, this measure is not valid due to sample degradation, making it unsuitable for DLS analysis. This is confirmed by the PDI value (1), indicating complete polydispersity. In other words, all particles in the sample have different sizes, making it impossible to obtain meaningful

data from DLS analysis. This degradation likely results from the freezing and thawing cycles, which can disrupt the lipid bilayer structure.

This study demonstrates the stability of LUVs over time, which is crucial for maintaining the efficacy of encapsulated therapeutics, ensuring reproducibility in research and meeting regulatory standards in industrial applications. Moreover, it is confirmed that freezing disrupts LUVs, and storing them at 4 °C is the optimal condition for preserving their integrity. However, exposure to ambient temperatures does not lead to substantial damage to LUVs, offering flexibility in storage conditions without compromising their stability.

5.1.3.2 Characterization with nanoparticles tracking analysis (NTA)

Nanoparticles tracking analysis method was also employed for the characterization of LUVs. This technique combines laser light scattering microscopy with a charge-coupled device (CCD) camera, allowing the visualization and recording of nanoparticles within a solution. Therefore, it is able to measure size, distribution and concentration of particles, and enables to observe and record live video of particles (39). This analytical approach was used for LUVs characterization and to assess the viability of concentrating them. In order to do so, 100 μL of LUVs from fraction 9 were diluted 3000 times in MiliQ water and injected into a Nanosight NS300 instrument from Malvern Panalytical. Measures were taken for 5 minutes in time ranges of 1 minute and 20 seconds, and detect threshold was set to 11. A concentration of 4.51e+08 ± 3.92e+07 particles/ml was obtained, and mean size of LUVs was 144.6 ± 6.0 nm (Figure 17). The concentration value is very high, which assures that our preparation process is efficient. Regarding to size, this measure was taken two months after their preparation, which confirms again their stability over time.

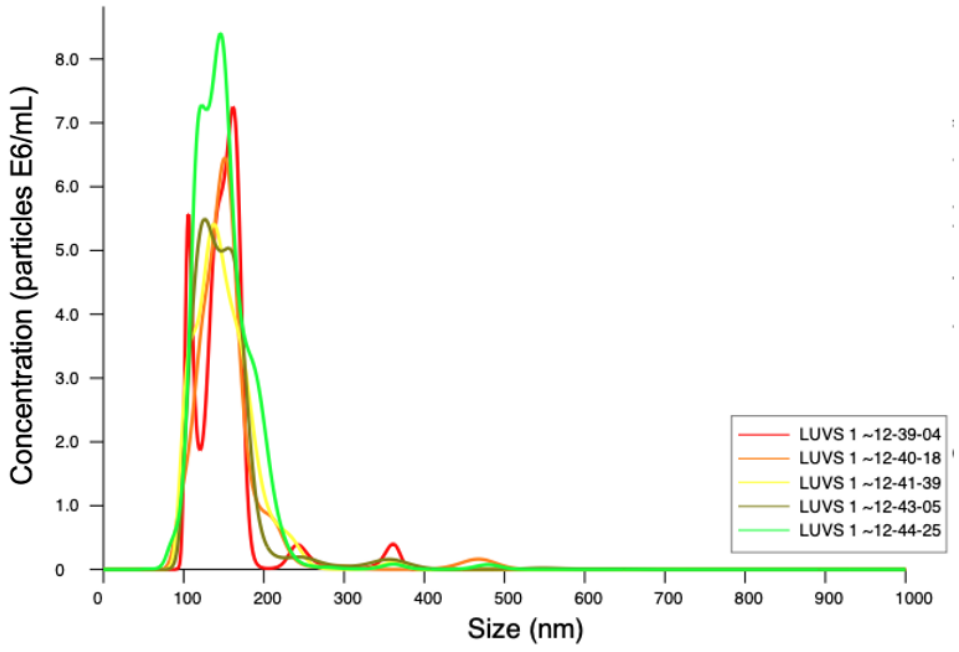

Figure 17. Concentration (particles E6/mL) by size (nm) of HRP-loaded LUVs measured with Nanosight.

5.1.3.2.1 Concentration of LUVs by centrifuge filtration units

A Microcon-10kDa centrifuge filtration unit was used to concentrate LUVs. The primary objective was to enhance the yield of LUVs, ensuring the feasibility of producing larger quantities suitable for commercialization. The column was loaded with 0.5 mL of LUVs and centrifuged twice for 10 minutes at 7000 rpm. Subsequently, the remaining fraction was diluted 3000 times in MiliQ water to measure its concentration using Nanosight. Identical conditions to those set previously were employed for this measure, and a concentration of 1.32e+09 ± 1.10e+08 particles/mL was obtained (Figure 18). This result signifies a substantial increase by about one order of magnitude, which indicates the effectiveness of the concentration method employed. Figure 19 shows LUVs observed by Nanosight before and after concentration.

On the other hand, the average size of the particles was 135.5 ± 0.3 nm, showing a decrease from the initial measurement before concentration. This reduction in size can be attributed to several factors, such as the removal of undesirable components during concentration.

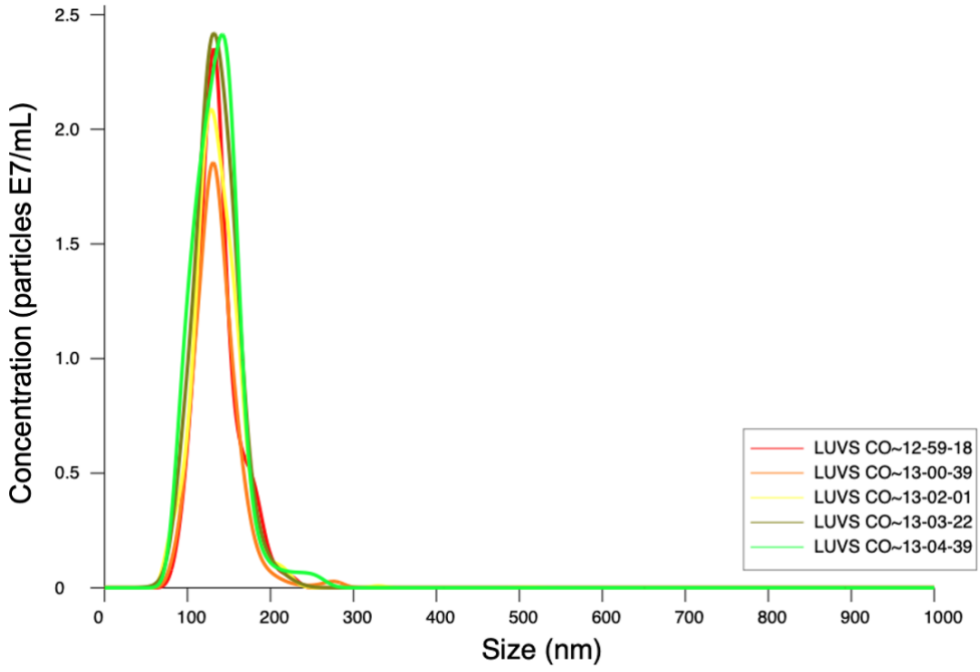

Figure 18. Concentration (particles E7/mL) by size (nm) of HRP-loaded LUVs after concentration, measured with Nanosight.

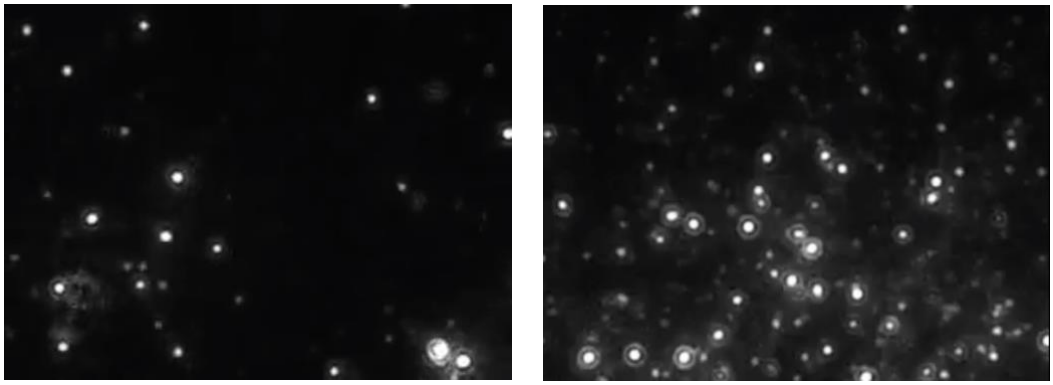

Figure 19. Nanosight images of HRP-loaded LUVs, before and after concentration.

5.1.3.3 Characterization with transmission electron microscopy (TEM)

TEM is a technique used to image the internal structure of solids utilizing a stream of high-energy electrons transmitted through the solid. A photographic image is captured from the electron flux once it has passed a thin sample of the specimen being examined (40). HRP-loaded LUVs were observed by TEM to visualize their structure and obtain detailed information about the morphology of these nanostructures (Figure 20).

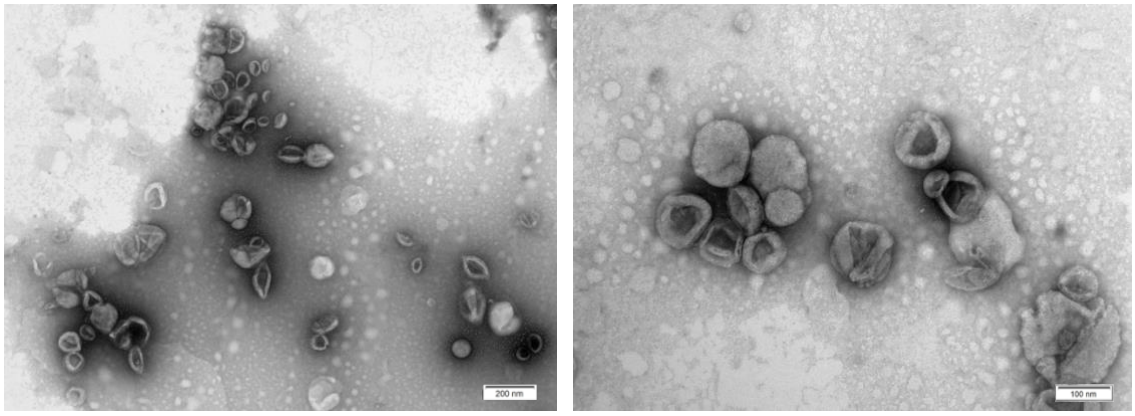

Figure 20. TEM images of HRP-loaded LUVs, with scale bars of 200 nm and 100 nm.

However, significant deformation and flattening of the vesicles were observed. This distortion can occur during the sample preparation process, particularly during the drying step required for TEM imaging. To overcome this issue and visualize the LUVs in their native state, cryo-TEM could be employed.

Cryo-TEM, or cryogenic transmission electron microscopy, involves flash-freezing the sample in a thin layer of vitreous ice. This rapid freezing process preserves the native structure of biological samples, including liposomes, without causing significant distortion or flattening. By imaging the sample at cryogenic temperatures, the lipid bilayers of the LUVs remain intact, allowing for high-resolution visualization of their morphology and

internal structure (41). Further experiments should take this into account in order to obtain a reliable image of the lipidic vesicles.

5.1.4 BCA Protein assay

In order to estimate the enzyme concentration inside the LUVs, BCA protein assays were performed. A calibration curve was plotted by measuring absorbances of HRP at concentrations from 5 μg/mL to 50 μg/mL (due to the dilution factor) in a spectrophotometer.

Then, 10 μL of LUVs from fraction 9 (milliliter 4.5 from the first batch of LUVs eluted from the Sepharose column) were mixed with 15 μL of PBS and 225 μL of kit reagents, and analyzed. The enzyme quantity within the nanoparticles was quantified using the equation derived from the calibration curve, coupled with the absorbance at 562 nm measured from the sample assay (Figure 21). Utilizing the calibration curve equation $y = 0{,}05316x + 0{,}0669$ (r2= 0.9989) and the absorbance value for the loaded liposome (A562 = 0.27 nm), the protein concentration in the nanoparticle solution was determined to be 96.25 μg/mL, after the appropriate corrections taking into account the dilution factor. A comparison graph of absorbance before and after mix with BCA reagents is shown in Figure 22.

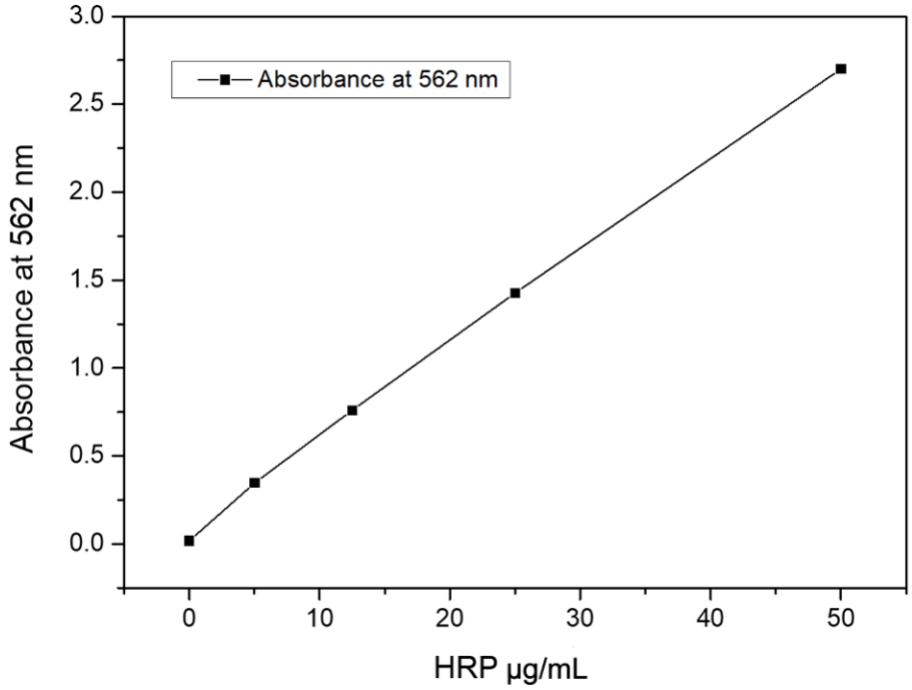

Figure 21. Calibration curve of HRP using the BCA protein assay, absorbance measured at 562 nm. Free HRP solution was diluted 25 times.

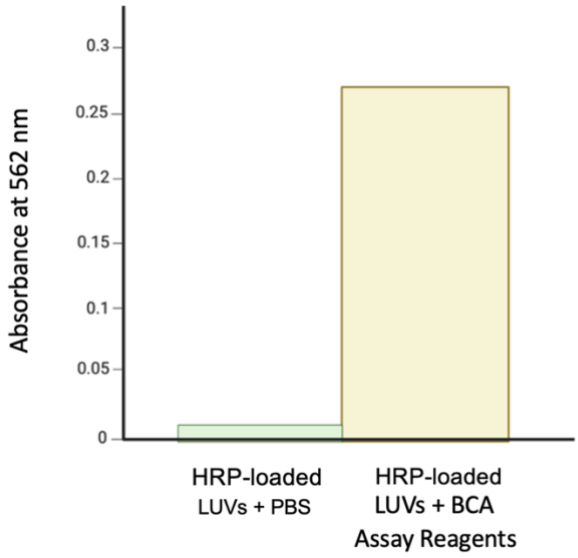

Figure 22. Absorbance of HRP-loaded LUVs in PBS (green); HRP-loaded LUVs absorbance at 562 nm after BCA assay (yellow).

Same procedure was followed for the estimation of the enzyme concentration inside LUVs from batch 2. The calibration curve vas plotted by measuring the absorbance of HRP at concentrations from 5 μg/mL to 50 μg/mL. Higher concentrations of HRP were not employed to avoid any signal saturation. The equation obtained from this calibration curve was the following one, with $R^2 = 0.9802$.

$$y = 0{,}2176x + 0{,}0535$$

Using this formula and taking into account the dilution factor, it was estimated that milliliter 4 expelled from the Sepharose column had an enzyme concentration of 144.86 μg/mL.

Control experiments were conducted in order to confirm the ability of the Sepharose 4B column to retain free protein molecules and separate them from liposomes. Free HRP was introduced into the column and the protein content of the eluted fractions was quantified. Likewise, HRP-loaded LUVs after extrusion were passed through the column, collecting and quantifying the eluted fractions. For both the free enzyme and LUVs, the volume placed into the column was of 1 mL, and the fractions collected were 12 fractions of 1 mL each.

Protein detection was carried out via a BCA assay using the PierceTM BCA Protein Assay Kit, with kit reagents mixed in a 1:50 ratio. Each fraction solution was combined with the reagents and incubated at 60°C for 30 minutes on a tube shaker. Subsequently, absorbance at 562 nm was measured for all fractions and a blank (225 μL of BCA reagents + 25 μL of PBS) and corresponding graphs (Figure 23) were generated.

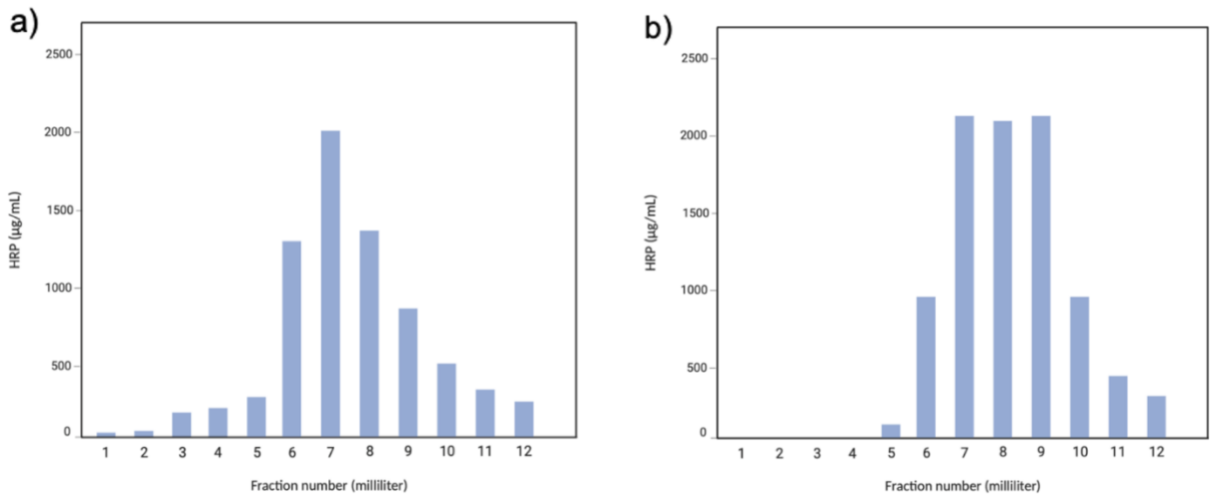

Figure 23. a) BCA assay of HRP-loaded LUVs after Sepharose 4B column purification **b)** BCA assay of free HRP (10 mg/mL) after Sepharose 4B column purification.

Analysis of absorbance readings revealed that protein detection, when passing free HRP through the column, started from milliliter 5. Characterization assays demonstrated that LUVs are found in milliliter 3 and 4. The absence of HRP in the fractions containing LUVs affirms that all peroxidase detected by the BCA assay in fractions 3 and 4 was encapsulated within the LUVs. This provides compelling evidence that the purification process effectively separates the free enzyme from the liposomes, ensuring that any detected protein is exclusively confined within the liposomal particles. Eluted fractions of free HRP as shown in Figure 24, where we can see by its orange color where the HRP is more concentrated, and how fractions 3 and 4 are peroxidase-free.

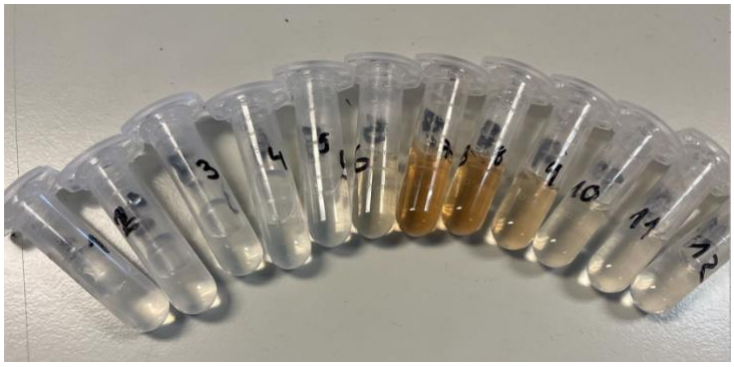

Figure 24. Eluted fractions of free HRP (10 mg/mL) after purification by SEC (Sepharose 4B).

5.1.5 Enzyme activity assay

Enzyme encapsulation could lead to changes in enzyme characteristics. Hence, it's crucial to assess enzyme activity post-conjugation with the nanoparticle. In order to determine if the HRP encapsulated within the LUVs retains its enzymatic activity, an

enzyme activity assay was conducted. In this assay, the substrate used was 2,2'-Azino-bis(3-Ethylbenzthiazoline-6-Sulfonic Acid) (ABTS). Upon interaction with HRP, hydrogen peroxide (H_2O_2) reacts with ABTS, producing a green-colored product (ABTS+), which can be quantified using a spectrophotometer at 418 nm.

Furthermore, validation of HRP encapsulation was also assessed through this experiment. LUVs were disrupted using dimethyl sulfoxide (DMSO), which allowed to release the encapsulated HRP from the vesicles. By comparing the enzymatic activity of disrupted LUVs with intact LUVs, we were able to determine the extent to which HRP was encapsulated.

These results (Figure 25) confirm that HRP-loaded LUVs remain active, as there is an increasement of absorbance at 418 nm with time. Notably, the slope of LUVs after treatment with DMSO exhibits a substantial increase compared to both the blank and the slope of LUVs before the disruption. This significant rise in enzymatic activity indicates efficient encapsulation and subsequent liberation of the enzyme.

When LUVs are not disrupted with DMSO, not all enzymatic activity may be measured. This limitation could stem from incomplete permeability of ABTS through the lipid bilayer of LUVs, hindering its interaction with encapsulated HRP. On the other hand, this represents an advantage for transporting the enzyme until its release inside the cell, avoiding off-target effects.

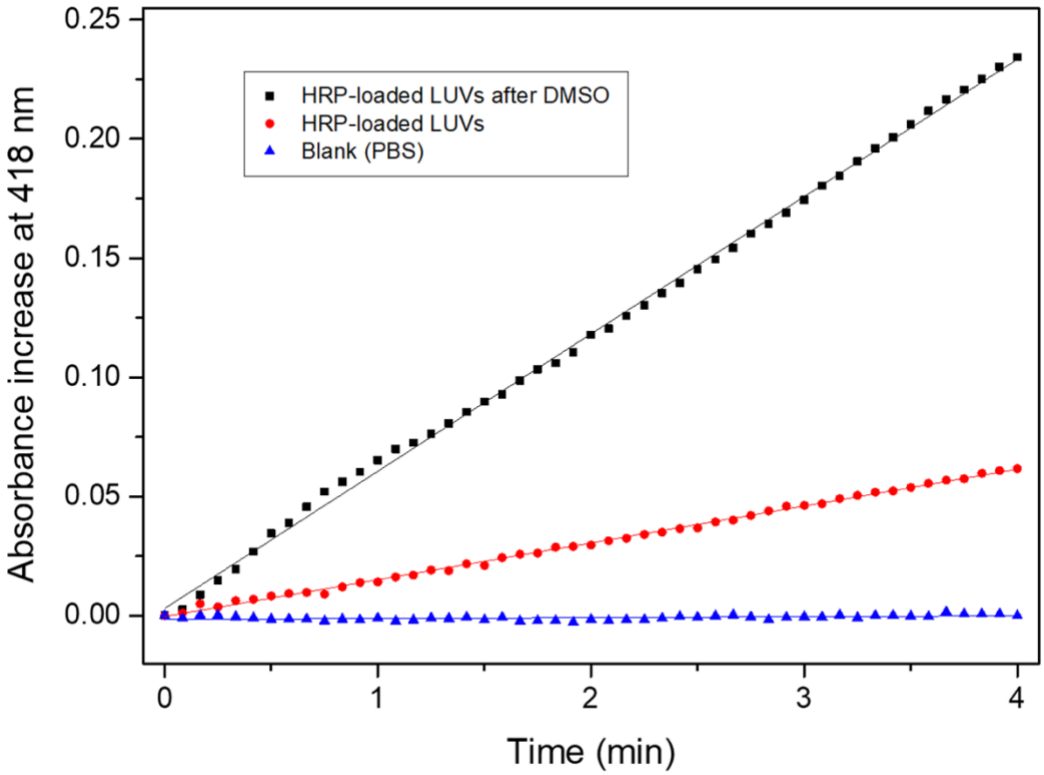

Figure 25. Monitoring of absorbance at 418 nm due to substrate transformation during enzymatic assay, upon addition of a blank of PBS (blue), HRP-loaded LUVs (red) and HRP-loaded LUVs after DMSO treatment (black).

Enzyme activity in units per milliliter (U/mL) was calculated as well to understand its efficacy post-encapsulation. The sample used for this purpose were LUVs after DMSO treatment, as the enzyme activity registered after disruption of the liposomes is higher and more accurate to the real activity of the enzyme within LUVs.

The following equation was followed to calculate enzymatic units:

$$\frac{U}{mL} = \frac{(\Delta - \Delta_{blank}) \times Total\ volume}{\varepsilon_{ABTS} \times Enzyme\ volume}$$

Where Δ denotes absorbance variation of the sample with time and Δ_{blank} denotes absorbance variation of the blank with time. Enzyme volume represents the volume of enzyme utilized in the assay, ε_{ABTS} represents the molar extinction coefficient of the ABTS product and total volume encompasses the total volume of the reaction mixture.

One unit (U) of HRP is defined as the amount of enzyme that oxidizes 1.0 μmol of ABTS per minute at pH 5.0 at 25 °C [i.e., H_2O_2 + ABTS → $2H_2O$ + oxidized ABTS]. Equations obtained from the enzyme activity assay were $y = 0.0004x - 0.0015$ for the blank and $y = 0.0576x + 0.0031$ for HRP-loaded LUVs after DMSO treatment. Based on this, and upon calculation, the enzymatic activity of the encapsulated HRP was determined to be 8.5×10^{-2} U/mL. This result aligns with the enzyme activity reported by previous studies about the use of HRP for cancer therapies (31).

Enzymatic activity of free HRP was monitored through time, conducting measurements at days 1, 14 and 21 after preparation of the HRP solution (Figure 26). The solid HRP was initially diluted with 1 milliliter of MilliQ water to achieve a concentration of 100 μg/ml. The same approach as previously was followed, using the same substrate ABTS and its interaction with H_2O_2 upon the action of HRP. The primary objective was to evaluate its stability and reliability to determine whether HRP maintains consistent functionality over time. Time of measurement was reduced to 0.3 min, as enzyme activity in day 1 reaches saturation in a shorter time.

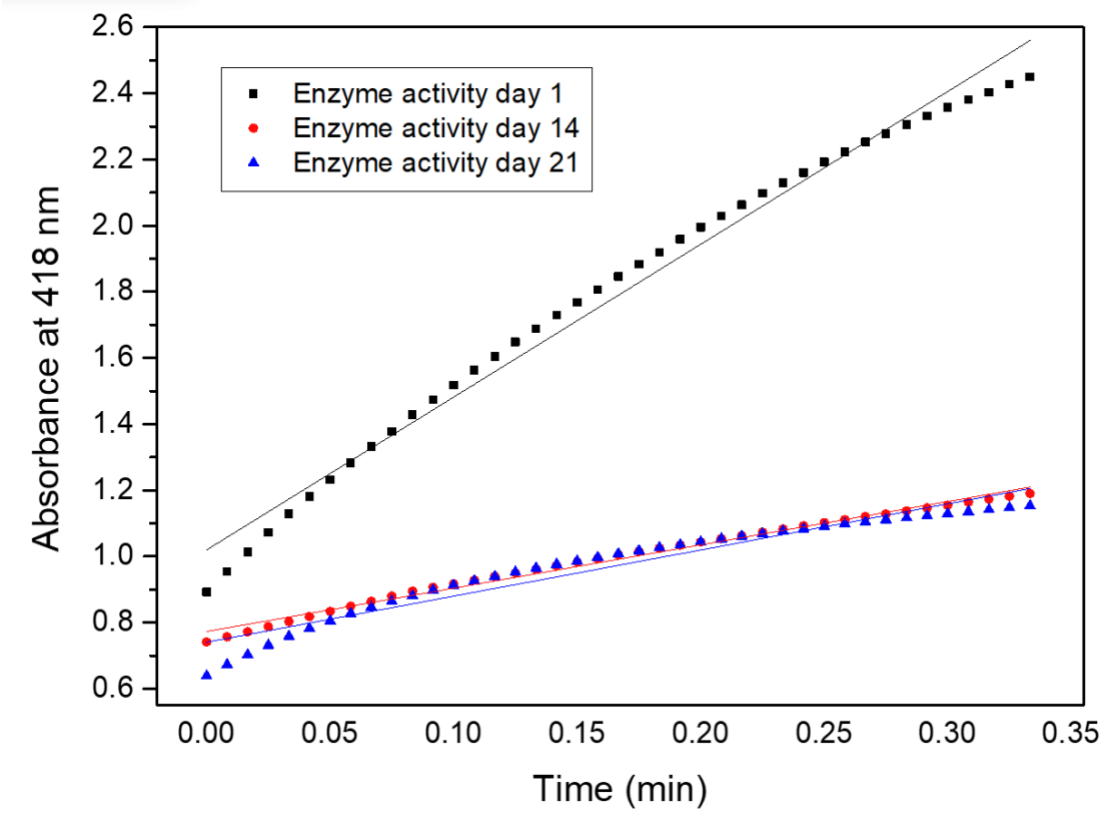

Figure 26. Monitoring of absorbance at 418 nm due to substrate transformation during enzymatic assay, upon addition of HRP in days 1 (black), 14 (red) and 21 (blue) after preparation.

It is observed that enzyme activity decreases within time. However, it still has a considerable activity. To ensure consistency and efficacy in therapeutic applications, it will be essential in future works to standardize the enzyme activity at specific time points. This involves determining the acceptable level of enzyme activity at different stages of storage and establishing protocols for assessing and verifying enzyme activity.

5.2 Evaluation of therapeutic effect on SK-Mel-103 cells

To explore the biocompatibility and the anticancer therapeutic potential of the HRP-loaded LUVs/IAA system, cell experiments were conducted utilizing SK-Mel-103 human melanoma cancer cells. A melanoma is a tumor produced by the malignant transformation of melanocytes. Melanocytes are derived from the neural crest; consequently, melanomas, although they usually occur on the skin, can arise in other locations where neural crest cells migrate, such as the gastrointestinal tract and brain. Melanoma stands as the type of skin cancer with a higher mortality and resistance to currently used treatments. SK-Mel-103 cells are commonly employed in cancer research due to their robust growth characteristics and relevance to melanoma (42). Table 1 shows a representation of the 96-wells plate utilized, along with the components and concentrations employed.

Table 1. 96-wells plate representation where HRP, IAA, LUVs, HRP-loaded LUVs, HRP/IAA and HRP-loaded LUVs/IAA, at different concentrations, were added to SK-Mel-103 cells.

CONTROL DMEM	Free HRP (50 μg/mL)	Free HRP (10 μg/mL)	Free IAA 1 mM	Free IAA 5 mM
		HRP(1 μg/mL)/IAA(1 mM)	HRP(5 μg/mL)/IAA(1 mM)	
		HRP(2 μg/mL)/IAA(1 mM)	HRP(10 μg/mL)/IAA(1 mM)	
	HRP-loaded LUVs 50 μg/mL	HRP(1 μg/mL)-loaded LUVs/IAA(1 mM)	HRP(5 μg/mL)-loaded LUVs/IAA(1 mM)	Empty
		HRP(2 μg/mL)-loaded LUVs/IAA(1 mM)	HRP(10 μg/mL)-loaded LUVs/IAA(1 mM)	
		HRP-loaded LUVs 10 μg/mL	Empty	

Firstly, the biocompatibility of HRP-loaded LUVs nanodevice was tested. SK-Mel-103 cells were incubated in the presence of HRP-loaded LUVs (10 μg/mL, 50 μg/mL). The findings indicated that melanoma cells exhibited tolerance to HRP-loaded LUVs at both concentrations following 24 hours of treatment (Figure 27). Consequently, the concentration range of 10 μg/mL to 50 μg/mL was validated as non-toxic.

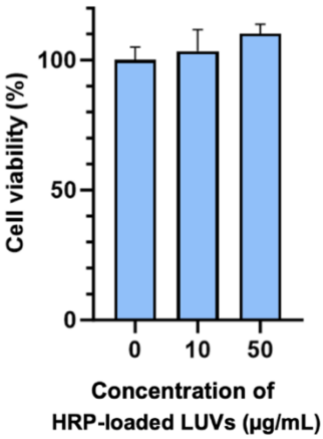

Figure 27. HRP-loaded LUVs for cell viability assessment in SK-Mel-103 melanoma cells.

Free HRP (10 µg/mL, 50 µg/mL) was measured on its own to assess its cytotoxicity, with an expectation of no significant reduction in cell viability. However, a slight decline in cell viability was observed (Figure 28), potentially due to intrinsic cytotoxicity of high concentrations of HRP, which may induce cellular stress responses or interfere with cellular processes. These measured concentrations are higher than the intended concentrations for use, as we wanted to establish a threshold. Lower concentrations of HRP were not tested as literature robustly suggested that it did not have any cytotoxic effects (27) (28) (29) (30) (31).

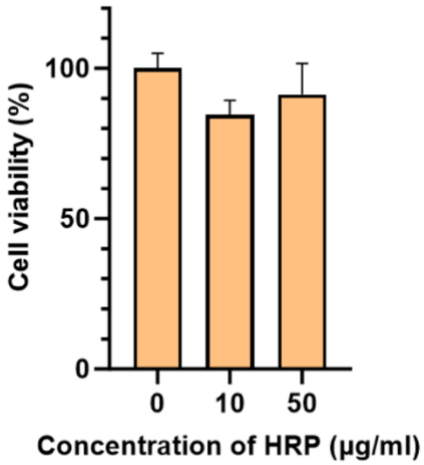

Figure 28. Free HRP for cell viability assessment in SK-Mel-103 melanoma cells.

Although higher concentrations of free HRP (10 µg/mL, 50 µg/mL) measured individually showed certain reduction in cell viability, same concentrations of HRP encapsulated into LUVs did not show any cytotoxicity (Figure 29). This can be attributed to their encapsulation, which confirms that this drug delivery system avoids off-target toxicity.

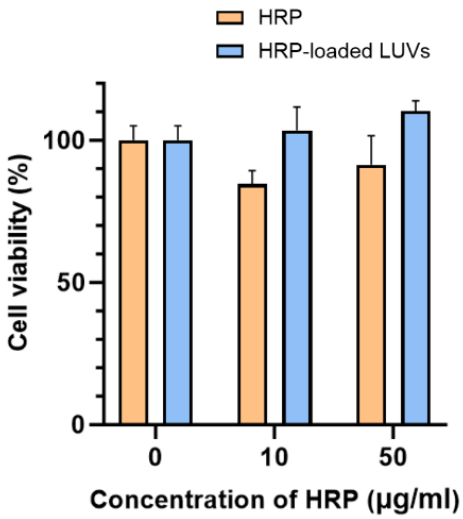

Figure 29. Free HRP and HRP-loaded LUVs for cell viability assessment in SK-Mel-103 melanoma cells.

Likewise, IAA was tested individually at concentrations of 1 mM and 5 mM and certain decrease in cell viability was observed (Figure 30). The explanation for this outcome might be similar to HRP. IAA itself could possess inherent cytotoxic properties at higher concentrations, leading to cellular stress and a reduction in viability. However, the reduction observed with 1 mM IAA does not significantly affect cell viability. Hence, future experiments should consider testing lower concentrations. Existing literature indicates that concentrations as 0.5 mM have no impact on cell viability (27) (28).

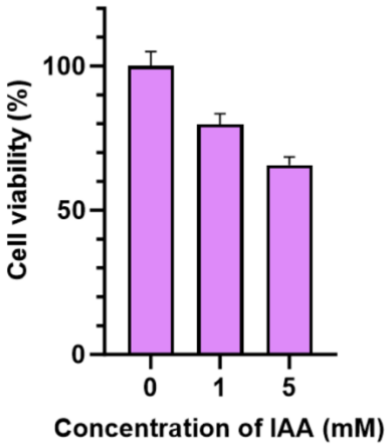

Figure 30. Free IAA for cell viability assessment in SK-Mel-103 melanoma cells.

In the following step, our aim was to assess the effectiveness of HRP-loaded LUVs combined with IAA (HRP-loaded LUVs/IAA) to induce melanoma cell death through an oxidative stress. The potential of HRP-loaded LUVs/IAA for EPT was investigated exposing cells to different concentrations of HRP-loaded LUVs (1 μg/mL, 2 μg/mL, 5 μg/mL, 10 μg/mL) and a permanent concentration of 1 mM of IAA. Following a 24 hours incubation period, cell viability was assessed using the WST-1 assay. We observed a slight decrease in cell viability for cells treated with HRP-loaded LUVs at concentrations of 1 μg/mL and 2 μg/mL (76%) (Figure 31). However, interestingly, no significant decrease in cell viability was observed for cells treated with HRP-loaded LUVs at concentrations of 5 μg/mL and 10 μg/mL. It's possible that the concentrations of 5 μg/mL and 10 μg/mL exceeded the threshold required for inducing cytotoxic effects, and the interaction between HRP-loaded LUVs and IAA might not have occurred optimally at these higher concentrations. Moreover, existing literature suggests that the optimal concentration of HRP is 1.2 μg/mL, as confirmed in previous studies (27) (28) (29) (30). However, we aimed to explore the effects of higher concentrations to assess their impact on cytotoxicity.

Additionally, in order to compare its effectiveness with HRP-loaded LUVs, we evaluated the efficacy of EPT using free HRP at equivalent concentrations (1 μg/mL, 2 μg/mL, 5 μg/mL, 10 μg/mL) with 1 mM of IAA as previously (Figure 31). The findings demonstrated a reduction in cell viability (70%). Results indicate that free HRP/IAA had a more pronounced reduction in cell viability compared to HRP-loaded LUVs/IAA.

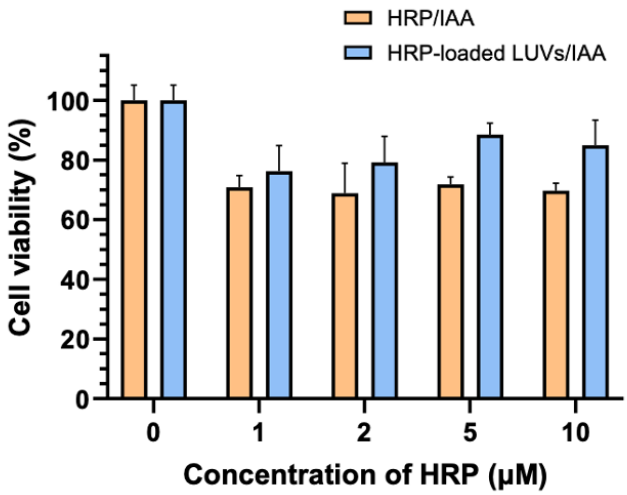

Figure 31. Free HRP/IAA and HRP-loaded LUVs/IAA for EPT cell viability assessment in SK-Mel-103 melanoma cells.

This outcome may be attributed to the release kinetics of cargo from liposomes or to differences in cellular uptake for free HRP and HRP-loaded LUVs system. However, the reduction of cell viability was only slight for both conditions, which suggests that further optimization of the experiment is necessary to enhance therapeutic efficacy. Probably, it would be necessary to extend the incubation time of cells exposed to HRP-loaded LUVs/IAA and HRP/IAA to induce more oxidative stress and allow a longer time for the reaction to occur, causing more cell death. This is particularly important in the case of HRP-loaded LUVs/IAA, since they need a period to be released through passive diffusion. Passive diffusion involves the gradual movement of HRP molecules from the liposome interior to the surrounding cellular environment. This process is slower compared to the direct exposure of cells to free HRP. Some literature suggests that incubation periods of 48 hours have yielded more favorable results in terms of therapeutic efficacy (30).

In addition, it would be helpful to measure reactive oxygen species (ROS) levels to confirm the oxidative stress induced by HRP-loaded LUVs/IAA. This could be achieved by employing ROS indicators such as CM-H2DCFDA stain, which allows for the monitoring of fluorescence upon interaction with ROS (39). By adding CM-H2DCFDA stain to cells treated with both free HRP/IAA and HRP-loaded LUVs/IAA, and subsequently assessing the fluorescence intensity, the generation of ROS could be quantified, providing insights into the levels of oxidative stress induced by HRP-loaded LUVs/IAA. Furthermore, it would be helpful to study the cellular uptake of HRP-loaded LUVs analyzing the internalization of the nanoparticles by TEM. High nanoparticle internalization is crucial for promoting prodrug activation by HRP inside tumor cells, amplifying the efficacy of enzyme-prodrug therapy (EPT). If the HRP-loaded LUVs internalization is not successfully reached, adjustments such as modifying liposomal size or surface properties might be necessary to enhance their cellular uptake.

However, we need to take into account that only a single assay for cell viability was conducted, primarily due to time constraints. Therefore, all obtained results must be corroborated through subsequent experiments to ensure their reliability and validity.

6. CONCLUSIONS

We report here the design, preparation, characterization and evaluation of a novel delivery system by incorporating horseradish peroxidase into liposomes (HRP-loaded LUVs) to perform enzyme prodrug therapy (EPT) in melanoma cancer cells. Large unilamellar vesicles (LUVs) were prepared by thin-film hydration method in a DOPC and cholesterol 70:30 molar ratio, and characterized by dynamic light scattering (DLS). Sodium fluoresceine was incorporated within LUVs (SF-loaded LUVs) to verify successful encapsulation through fluorometer measurements, and characterized by DLS. Once it was confirmed, horseradish peroxidase was encapsulated into LUVs (HRP-loaded LUVs), and characterized by DLS, nanoparticles tracking analysis (NTA) and transmission electron microscopy (TEM).

Characterization showed that size and zeta potential of LUVs were in the expected ranges for stability and cellular uptake (9) (43). Furthermore, stability studies by DLS revealed that HRP-loaded LUVs remained stable throughout the 28-day study period at 4°C, consistent with typical storage conditions for lipid-based formulations. Regarding enzyme activity, results confirmed that HRP-loaded LUVs remain active after encapsulation. Moreover, the obtained enzyme activity value aligns with those reported in literature (31). On the other hand, LUVs concentration was achieved, signifying a potential advantage for LUVs storage and commercialization.

Biocompatibility experiments demonstrated that HRP-loaded LUVs are well tolerated by cells. Reductions in cell viability were observed when treating cancer cells with HRP-loaded LUVs and IAA, yet future optimization of incubation times are needed to better evaluate their therapeutic effect. This opens the possibility to study the anticancer effect of HRP-loaded LUVs in combination with IAA (via oxidative stress) in future experiments.

Overall, this project has successfully developed HRP-loaded LUVs, validating effective encapsulation, stability and biocompatibility. Reductions in cell viability were observed through this system, although future optimization strategies are needed to enhance therapeutic effect. This research aligns with the Sustainable Development Goals (SDG), specifically with Health and Well-being (SDG 3), as it provides promising perspectives for cancer treatment with minimized side effects, enhancing patient well-being. Furthermore, the utilization of nanomedicine and targeted drug delivery systems support Industry, Innovation and Infrastructure goal (SDG 9) by promoting modern approaches to cancer therapy. This work contributes to advance knowledge in the area of nanomedicine concerning cancer therapies, representing promising outcomes for further research in this field.

7. BIBLIOGRAPHY

1. Yusuf A, Almotairy ARZ, Henidi H, Alshehri OY, Aldughaim MS. Nanoparticles as Drug Delivery Systems: A Review of the Implication of Nanoparticles' Physicochemical Properties on Responses in Biological Systems. *Polymers*. 2023;15(7):1596.

2. Yao Y, Zhou Y, Liu L, Xu Y, Chen Q, Wang Y, et al. Nanoparticle-Based Drug Delivery in Cancer Therapy and Its Role in Overcoming Drug Resistance. *Front Mol Biosci*. 2020;7:193.

3. Patra JK, Das G, Fraceto LF, Campos EVR, Rodriguez-Torres MDP, Acosta-Torres LS, et al. Nano based drug delivery systems: recent developments and future prospects. *J Nanobiotechnology.* 2018;16(1):71.

4. Nirmala MJ, Kizhuveetil U, Johnson A, G B, Nagarajan R, Muthuvijayan V. Cancer nanomedicine: a review of nano-therapeutics and challenges ahead. *RSC Adv.* 2023;13(13):8606-29.

5. O'Brien MER, Wigler N, Inbar M, Rosso R, Grischke E, Santoro A, et al. Reduced cardiotoxicity and comparable efficacy in a phase IIItrial of pegylated liposomal doxorubicin HCl(CAELYX™/Doxil®) versus conventional doxorubicin forfirst-line treatment of metastatic breast cancer. *Ann Oncol*. 2004;15(3):440-9.

6. Li W, Zhang H, Assaraf YG, Zhao K, Xu X, Xie J, et al. Overcoming ABC transporter-mediated multidrug resistance: Molecular mechanisms and novel therapeutic drug strategies. *Drug Resist Updat.* 2016;27:14-29.

7. Alavi M, Hamidi M. Passive and active targeting in cancer therapy by liposomes and lipid nanoparticles. *Drug Metab Pers Ther*. 2019;34(1).

8. Carmeliet P, Jain RK. Angiogenesis in cancer and other diseases. *Nature*. 2000; 407(6801):249-57.

9. Lombardo D, Kiselev MA. Methods of Liposomes Preparation: Formation and Control Factors of Versatile Nanocarriers for Biomedical and Nanomedicine Application. *Pharmaceutics.* 2022;14(3):543.

10. Murthy SK. Nanoparticles in modern medicine: state of the art and future challenges. *Int J Nanomedicine.* 2007;2(2):129-41.

11. Lombardo D, Kiselev MA. Methods of Liposomes Preparation: Formation and Control Factors of Versatile Nanocarriers for Biomedical and Nanomedicine Application. *Pharmaceutics.* 2022;14(3):543.

12. Boban Z, Mardešić I, Jozić SP, Šumanovac J, Subczynski WK, Raguz M. Electroformation of Giant Unilamellar Vesicles from Damp Lipid Films Formed by Vesicle Fusion. *Membranes.* 2023;13(3):352.

13. Gabizon A, Shmeeda H, Barenholz Y. Pharmacokinetics of Pegylated Liposomal Doxorubicin: Review of Animal and Human Studies. *Clin Pharmacokinet.* 2003;42(5):419-36.

14. Gabizon AA. Pegylated Liposomal Doxorubicin: Metamorphosis of an Old Drug into a New Form of Chemotherapy. *Cancer Invest*. 2001;19(4):424-36.

15. Han B, Yang Y, Chen J, Tang H, Sun Y, Zhang Z, et al. Preparation, Characterization, and Pharmacokinetic Study of a Novel Long-Acting Targeted Paclitaxel Liposome with Antitumor Activity. *Int J Nanomedicine* 2020; Volume 15:553-71.

16. De La Fuente M, Lombardero L, Gómez-González A, Solari C, Angulo-Barturen I, Acera A, et al. Enzyme Therapy: Current Challenges and Future Perspectives. *Int J Mol Sci.* 2021;22(17):9181.

17. Hennigan JN, Lynch MD. The past, present, and future of enzyme-based therapies. *Drug Discov Today.* 2022;27(1):117-33.

18. Zhang H, Lv P, Jiang J, Liu Y, Yan R, Shu S, et al. Advances in developing ACE2 derivatives against SARS-CoV-2. *Lancet Microbe*. 2023;4(5):e369-78.

19. De La Fuente M, Lombardero L, Gómez-González A, Solari C, Angulo-Barturen I, Acera A, et al. Enzyme Therapy: Current Challenges and Future Perspectives. *Int J Mol Sci.* 2021;22(17):9181.

20. Spadiut O, Herwig C. Production and purification of the multifunctional enzyme horseradish peroxidase. *Pharm Bioprocess*. 2013;1(3):283-95.

21. Krainer FW, Glieder A. An updated view on horseradish peroxidases: recombinant production and biotechnological applications. *Appl Microbiol Biotechnol.* 2015;99(4):1611-25.

22. Neumann B, Wollenberger U. Electrochemical Biosensors Employing Natural and Artificial Heme Peroxidases on Semiconductors. *Sensors.* 2020;20(13):3692.

23. Humer D, Spadiut O. Enzyme prodrug therapy: cytotoxic potential of paracetamol turnover with recombinant horseradish peroxidase. *Monatshefte Für Chem - Chem Mon.* 2021;152(11):1389-97.

24. Kim DS, Jeon SE, Park KC. Oxidation of indole-3-acetic acid by horseradish peroxidase induces apoptosis in G361 human melanoma cells. *Cell Signal.* 2004;16(1):81-8.

25. Braun S, Gaza N, Werdehausen R, Hermanns H, Bauer I, Durieux ME, et al. Ketamine induces apoptosis via the mitochondrial pathway in human lymphocytes and neuronal cells. *Br J Anaesth.* 2010;105(3):347-54.

26. Salmon TB, Evert BA, Song B, Doetsch PW. Biological consequences of oxidative stress-induced DNA damage in Saccharomyces cerevisiae. *Nucleic Acids Res.* 2004;32(12):3712-23.

27. Vivo-Llorca G, Morellá-Aucejo Á, García-Fernández A, Díez P, Llopis-Lorente A, Orzáez M, et al. Horseradish Peroxidase-Functionalized Gold Nanoconjugates for Breast Cancer Treatment Based on Enzyme Prodrug Therapy. *Int J Nanomedicine.* 2022;Volume 17:409-22.

28. Humer D, Furlanetto V, Schruef AK, Wlodarczyk A, Kuttke M, Divne C, et al. Potential of unglycosylated horseradish peroxidase variants for enzyme prodrug cancer therapy. *Biomed Pharmacother.* 2021;142:112037.

29. Bonifert G, Folkes L, Gmeiner C, Dachs G, Spadiut O. Recombinant horseradish peroxidase variants for targeted cancer treatment. *Cancer Med.* 2016;5(6):1194-203.

30. Folkes LK, Wardman P. Oxidative activation of indole-3-acetic acids to cytotoxic species— a potential new role for plant auxins in cancer therapy11Abbreviations: IAA, indole-3-acetic acid; HRP, horseradish peroxidase; TBA, thiobarbituric acid; MPO, myeloperoxidase; MOI, 3-methylene-2-oxindole; BSO, buthionine sulphoximine; GSH, glutathione; CEA, carcinoembryonic antigen; ADEPT, antibody directed enzyme prodrug therapy; PDEPT, polymer directed enzyme prodrug therapy; GDEPT, gene directed enzyme prodrug therapy; and PEG, polyethylene glycol. *Biochem Pharmacol.* 2001;61(2):129-36.

31. Vivo-Llorca G, Morellá-Aucejo Á, García-Fernández A, Díez P, Llopis-Lorente A, Orzáez

M, et al. Horseradish Peroxidase-Functionalized Gold Nanoconjugates for Breast Cancer Treatment Based on Enzyme Prodrug Therapy. *Int J Nanomedicine.* 2022;Volume 17:409-22.

32. Chibowski E, Szcześ A. Zeta potential and surface charge of DPPC and DOPC liposomes in the presence of PLC enzyme. *Adsorption*. 2016;22(4-6):755-65.

33. Danaei M, Dehghankhold M, Ataei S, Hasanzadeh Davarani F, Javanmard R, Dokhani A, et al. Impact of Particle Size and Polydispersity Index on the Clinical Applications of Lipidic Nanocarrier Systems. *Pharmaceutics.* 2018;10(2):57.

34. Danaei M, Dehghankhold M, Ataei S, Hasanzadeh Davarani F, Javanmard R, Dokhani A, et al. Impact of Particle Size and Polydispersity Index on the Clinical Applications of Lipidic Nanocarrier Systems. *Pharmaceutics*. 2018;10(2):57.

35. Kepekçi RA, Yener İlçe B, Demir Kanmazalp S. Plant-derived biomaterials for wound healing. En: Studies in Natural Products Chemistry [Internet]. *Elsevier;* 2021. p. 227-64.

36. Németh Z, Csóka I, Semnani Jazani R, Sipos B, Haspel H, Kozma G, et al. Quality by Design-Driven Zeta Potential Optimisation Study of Liposomes with Charge Imparting Membrane Additives. *Pharmaceutics*. 2022;14(9):1798.

37. Kim YM, Chang WJ, Koo YM. On-line recovery of large molecules from mixture solution using semi-continuous size exclusion chromatography. Progress in Biotechnology. *Elsevier;* 2000 p. 21-4.

38. Ashley J, Manikova P. Fluorescent sensors. En: Fundamentals of Sensor Technology. *Elsevier;* 2023 p. 147-61.

39. Filipe V, Hawe A, Jiskoot W. Critical Evaluation of Nanoparticle Tracking Analysis (NTA) by NanoSight for the Measurement of Nanoparticles and Protein Aggregates. *Pharm Res.* 2010;27(5):796-810.

40. Stachowiak GW, Batchelor AW, Stachowiak GB. Surface Micrography and Analysis. En: Tribology Series [Internet]. *Elsevier;* 2004. p. 165-220.

41. Almgren M, Edwards K, Karlsson G. Cryo transmission electron microscopy of liposomes and related structures. *Colloids Surf Physicochem Eng Asp.* 2000;174(1-2):3-21.

42. Matias M, Pinho JO, Penetra MJ, Campos G, Reis CP, Gaspar MM. The Challenging Melanoma Landscape: From Early Drug Discovery to Clinical Approval. *Cells.*2021;10(11):3088.

43. Németh Z, Csóka I, Semnani Jazani R, Sipos B, Haspel H, Kozma G, et al. Quality by Design-Driven Zeta Potential Optimisation Study of Liposomes with Charge Imparting Membrane Additives. *Pharmaceutics.* 2022;14(9):1798.